water

MDPI

Article

A Verification of Seismo-Hydrogeodynamic Effect Typifications Recorded in Wells on the Kamchatka Peninsula: The 3 April 2023 Earthquake, M_w = 6.6, as an Example

Galina Kopylova * and Svetlana Boldina

Laboratory of Geophysical Research, Kamchatka Branch of the Geophysical Survey of the Russian Academy of Sciences (KB GS RAS), 683006 Petropavlovsk-Kamchatsky, Russia; boldina@emsd.ru
* Correspondence: gala@emsd.ru

Abstract: Long-term observations in wells make it possible to study changes in groundwater pressure/level during individual earthquakes (seismo-hydrogeodynamic effects—SHGEs) over a wide range of periods of their manifestation. Information on the morphological features and durations of the SHGEs together with data on earthquake parameters form the basis for creating the unique typifications of SHGEs for individual observation wells. With reliable verification, such SHGE typifications provide the practical use of well observation data to predict strong earthquakes and assess their impact on groundwater. During long-term (1996–2022) precision observations of pressure/water level variations in wells of the Petropavlovsk–Kamchatsky test site (Kamchatka Peninsula, northwest Pacific seismic belt), SHGE typifications describing the manifestations of various types of SHGEs at the earthquakes in ranges of magnitudes M_w = 5.0–9.1 and epicentral distances d_e = 80–14,600 km were developed. At the same time, the issue of verifying created SHGE typifications for individual wells in relation to the strongest and closest earthquakes, accompanied by noticeable tremors in the observation area, is relevant. On 3 April 2023, an earthquake, M_w = 6.6 (EQ), occurred at an epicentral distance d_e = 67–77 km from observation wells. Various changes in the groundwater pressure/level were recorded in the wells: oscillations and other short-term and long-term effects of seismic waves, coseismic jumps in water pressure caused by a change in the static stress state of water-bearing rocks during the formation of rupture in the earthquake source, and supposed hydrogeodynamic precursors. The EQ was used to verify the SHGE typifications for wells YuZ-5 and E-1 with the longest observation series of more than 25 years. In these wells, the seismo-hydrogeodynamic effects recorded during the EQ corresponded to the previously observed SHGE during the two strongest earthquakes with M_w = 7.2, d_e = 80 km and M_w = 7.8, d_e = 200 km. This correspondence is considered an example of the experimental verification of previously created SHGE typifications in individual wells in relation to the most powerful earthquakes in the wells' area. Updated SHGE typifications for wells E-1 and YuZ-5 are presented, showing the patterns of water level/pressure changes in these wells depending on earthquake parameters and thereby increasing the practical significance of well observations for assessing earthquake consequences for groundwater, searching for hydrogeodynamic precursors and forecasting strong earthquakes. The features of the hydrogeodynamic precursor manifesting in the water level/pressure lowering with increased rates in well E-1 before earthquakes with M_w ≥ 5.0 at epicentral distances of up to 360 km are considered. A retrospective statistical analysis of the prognostic significance of this precursor showed that its use for earthquake forecasting increases the efficiency of predicting earthquakes with M_w ≥ 5.0 by 1.55 times and efficiency of predicting earthquakes with M_w

Academic Editors: Paolo Madonia and Juan José Durán

Received: 24 October 2024
Revised: 15 January 2025
Accepted: 6 February 2025
Published: 21 February 2025

Citation: Kopylova, G.; Boldina, S. A Verification of Seismo-Hydrogeodynamic Effect Typifications Recorded in Wells on the Kamchatka Peninsula: The 3 April 2023 Earthquake, M_w = 6.6, as an Example. *Water* **2025**, *17*, 634. https://doi.org/10.3390/w17050634

≥ 5.8 by 2.34 times compared to random guessing. This precursor was recorded during the 92 days before the EQ and was identified in real time with the issuance of an early prognostic conclusion on the possibility of a strong earthquake to the Kamchatka branch of the Russian Expert Council for Earthquake Forecasting.

Keywords: well; groundwater pressure; earthquake; typification of seismo-hydrogeodynamic effects; earthquake forecast; Kamchatka Peninsula

1. Introduction

For decades, the geosciences have been interested in studying the impacts of earthquakes on the natural environment, including on underground water. The variety of phenomena observed in pressure, level, discharge, temperature, and hydrogeochemistry changes in underground water during strong earthquakes do not yet have an exhaustive explanation regarding the relationship between different types of such phenomena and earthquake parameters. Of particular interest is the experimental study of the hydrogeological precursors of strong earthquakes on data from long-term precision observations in wells.

A detailed description of the diversity of seismo-hydrogeological effects, including observation data on wells in various regions of the Earth, is given in the monographs in [1,2]. At the same time, the authors note the need for further well observations in seismically active regions during strong earthquakes, especially at the stages of their preparation. This is due to the fact that the possibility of deriving the timely diagnostics of hydrogeodynamic and hydrogeochemical precursors for their use in forecasting strong earthquakes still remains controversial.

This paper examines changes in groundwater pressure in observation wells located in the east of the Kamchatka Peninsula (Figure 1) during an earthquake with a magnitude of M_w = 6.6 that occurred on 3 April 2023 (hereinafter, EQ) at an epicentral distance of d_e = 67–77 km in comparison with seismo-hydrogeodynamic effects (SHGEs) recorded in these wells during other previously occurring earthquakes with a wide range of magnitudes and epicentral distances, detailed descriptions of which were given in the authors' previous publications.

When a strong earthquake occurs near the area of precision observations of groundwater parameters in wells, a unique opportunity arises for a detailed study of the impact of seismicity on groundwater. To study such phenomena, it is preferable to use deep wells in conditions without man-made influence [3]. If this condition is met, as in the case of observation wells in Kamchatka, each strong earthquake, together with reliably diagnosed changes in groundwater parameters, both preceding the earthquake and associated with its implementation, represents valuable scientific facts that form the basis for studying the influence of seismicity on underground aquifers and the possibility of using hydrogeological precursors for forecasting strong earthquakes.

During the entire observation period at the Kamchatka wells in 1996–2023, digital equipment was used [4,5], allowing for the diagnosis of SHGE in the range of periods from seconds to minutes to hours to days and tens of days (Section 3). The seismo-hydrogeodynamic effects in pressure/water level changes recorded in observation wells during the EQ are presented in Section 4. A comparison was made of the SHGE detected in wells E-1 and YuZ-5 during the EQ with previously recorded SHGE in these wells during the most dangerous and nearby earthquakes. The purpose of such a comparison was to verify previously created typifications of the SHGE for individual wells, especially during strong local earthquakes, which occur rarely.

The refinement of the set of SHGEs in individual wells during a strong earthquake increases the practical significance of well observations for seismic forecasting and assessing the impact of such events on monitored aquifers and the technical condition of observation wells.

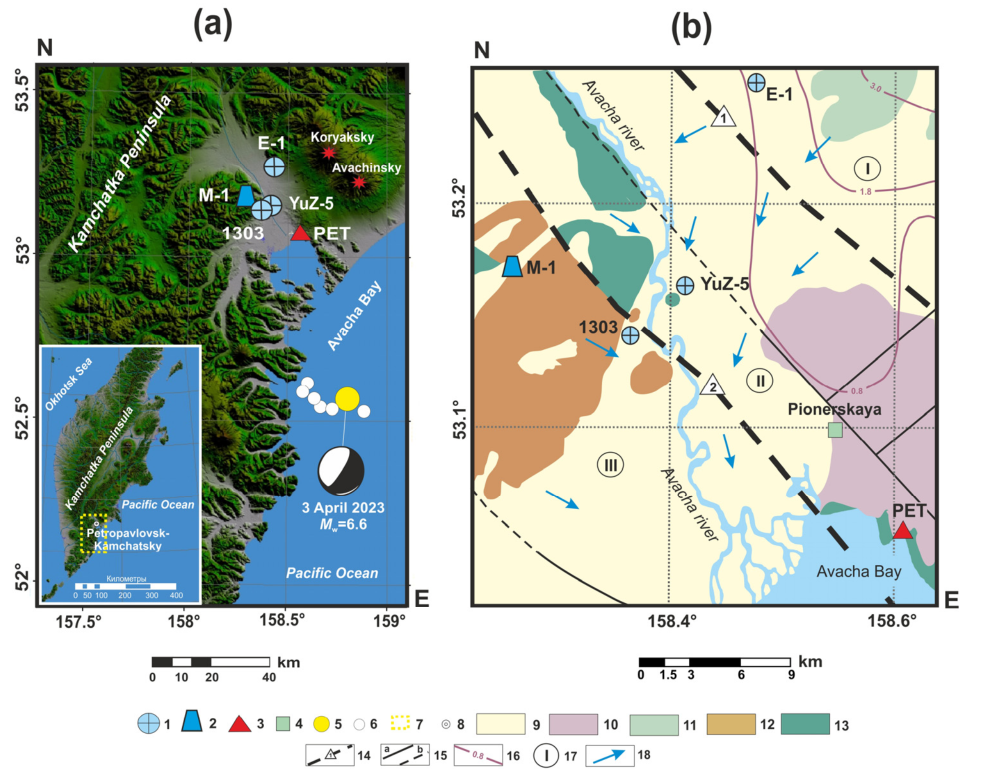

Figure 1. Location observation wells (Table 1) on the territory of Petropavlovsk–Kamchatsky geodynamic test site (shown with a yellow dotted line in the inset), geologic setting, epicenter and focal mechanism of 3 April 2023 earthquake, M_w = 6.6 (Table 2) and the epicenters of major aftershocks (according to data of NEIS (https://earthquake.usgs.gov/earthquakes/search (accessed on 20 January 2024)), GlobalCMT (https://www.globalcmt.org (accessed on 20 January 2024)) and the Kamchatka Branch of the Geophysical Survey of the Russian Academy of Sciences (http://sdis.emsd.ru/info/earthquakes/catalogue.php (accessed on 20 January 2024)). (**a**) Location of observation wells: 1—piezometric well, 2—flowing well, 3—Petropavlovsk (PET) seismic station, 7—Petropavlovsk–Kamchatsky geodynamic test site (inset), 8—Petropavlovsk–Kamchatsky city (inset). (**b**) Geological environment according to [6–8] with author's additions: 4—weather station, 5—main event epicenter, 6—aftershock epicenters, 9–13—geological formations (9—Quaternary sedimentary deposits, 10—Quaternary volcanogenic deposits, 11—Quaternary lavas of modern volcanoes, 12—Neogene volcanogenic–sedimentary rocks, 13—Late Cretaceous metamorphosed volcanogenic–sedimentary rocks), 14—regional faults (1—Avachinsky, 2—Petropavlovsky), 15—faults (a—established, b—assumed), 16—depth to the metamorphosed basement in km, 17—tectonic structures (I—Avacha volcano-tectonic depression, II—Petropavlovsky horst, III—Nachikinskaya zone of fold-block dislocations), 18—direction of regional underground runoff.

Particular attention in the work is given to the description of the hydrogeodynamic precursor (HGP) manifested in the water level/pressure changes in well E-1. The paper provides updated retrospective estimates of the prognostic significance of this precursor for the entire observation period, showing the possibility of its use for predicting earthquakes with magnitudes $M_w \geq 5.0$ at epicentral distances of up to 360 km (see Section 3.1.1).

Since 2002, based on the detection or absence of this hydrogeodynamic precursor in real time, weekly reports on the possibility of a strong earthquake in the area of the Petropavlovsk–Kamchatsky geodynamic test site have been compiled and transmitted to the Kamchatka branch of the Russian Expert Council for Earthquake Forecasting (KB REC) [9]. Before the EQ, the hydrogeodynamic precursor in pressure and water level changes was diagnosed with the issuance of a prognostic conclusion. The earthquake that occurred on 3 April 2023, is in satisfactory agreement in magnitude, time and location with the early forecast based on observations of the hydrogeodynamic precursor in well E-1.

Section 5 presents diagrams of the refined SHGE typifications for wells YuZ-5 and E-1, taking into account the observation data during the earthquake of 3 April 2023, and also discusses the issues of creating and using SHGE typifications when conducting observations at wells in order to search for earthquake precursors and study the impact of seismicity on groundwater.

Table 1. Observation wells, Kamchatka Peninsula.

Wells	Coordinates	Precision observations Start Date (Precision observations Duration *)	Depth, m Open Interval, m	Lithology: Age, Composition	Water Level Depth, h, m Discharge Rate, q, L/s;	Water Temperature, °C	Water Mineralization, g/L	Water Type	Gas Composition
YuZ-5	53.17° N 158.41° E	Sept 1997 (26.4 years)	800 310–800	K2, mudstone, shale	piezometric h = 1.5	14	0.45	HCO_3–SO_4–Na–Ca	dissolved gas, N_2
E-1	53.26° N 158.48° E	Jan 1996 (28 years)	665 625–645	N, Tuffs	piezometric h = 27	10	1.5	Cl–HCO_3–Na	free gas, N_2–CH_4
1303	53.14° N 158.36° E	April 2021 (2.8 years)	717 517–717	N, Tuffs	piezometric h = 25	14	0.67	HCO_3–SO_4–Na	dissolved gas, N_2
M-1	53.18° N 158.28° E	July 2020 (3.6 years)	600 310–313 407–410 553–556	N, Tuffs	self-flowing, q = 1.5	16	0.25	SO_4–Ca–Na	dissolved gas, N_2

Notes: * Number of years as of 1 February 2024.

Table 2. Earthquake data (https://www.globalcmt.org; https://earthquake.usgs.gov; https://glob.emsd.ru (accessed on 20 January 2024)).

EQ Date	EQ Time	EQ Hypocenter Coordinates			M_w	Earthquake Source Mechanism According to CMT https://www.globalcmt.org (accessed on 20 January 2024)				Earthquake Source Dimensions ****		Movement Along the Rupture *****
		N, (°)	E, (°)	H, km		Scalar Seismic Moment M_0, N × m × 10^{20}	Strike, (°)	Dip, (°)	Rake, (°)	W, m	L, m	U, m
3 April 2023	03:06:59	52.58	158.76	95	6.6 * 6.5 ** 6.6 ***	0.1	215 (104)	86 (10)	80 (159)	15,798	41,210	0.46

Notes: * Magnitude of the earthquake according to the catalog https://www.globalcmt.org (accessed on 20 January 2024). ** Magnitude of the earthquake according to the catalog https://earthquake.usgs.gov (accessed on 20 January 2024). *** Magnitude of the earthquake according to the catalog https://glob.emsd.ru (accessed on 20 January 2024). **** L, length along the strike, and W, width along the dip, were estimated from magnitude M_w = 6.6 according to the following formulas: $\lg L = 0.440 \times M_w - 1.289$ and $\lg W = 0.401 \times M_w - 1.448$ [10]. ***** The amount of movement along the rupture U was found from scalar seismic moment M_0, in $U = M_0/S \times \mu$, where $S = L \times W$ is the rupture area, and $\mu = 30 \times 10^9$ N/m^2 is the shear modulus of elastic medium.

2. Wells, Equipment, Data Processing

The Kamchatka Peninsula is located in the northwestern part of the Pacific seismic belt, at the junction between the Pacific oceanic plate and the continental Eurasian and North American plates. Here, seismic activity reaches the maximum level on the Earth and strong earthquakes with magnitudes up to 8–9 occur with a recurrence rate of the first hundred years [11,12]. Here, at the Petropavlovsk–Kamchatsky geodynamic test site (Figure 1a), precision observations of groundwater pressure are carried out in four deep wells in order to study seismo-hydrogeodynamic phenomena. The geological and hydrogeological environment of the wells' area (Figure 1b) is given in [5]. Observations were carried out by the Kamchatka branch of the Geophysical Survey of the Russian Academy of Sciences (KB GS RAS).

Well data are presented in Table 1 and Figure 2. The YuZ-5, E-1 and 1303 wells are piezometric with the water level at depths of 1.5–27 m below the Earth's surface. The M-1 well is self-flowing with a water flow rate of 1.5 *L*/s.

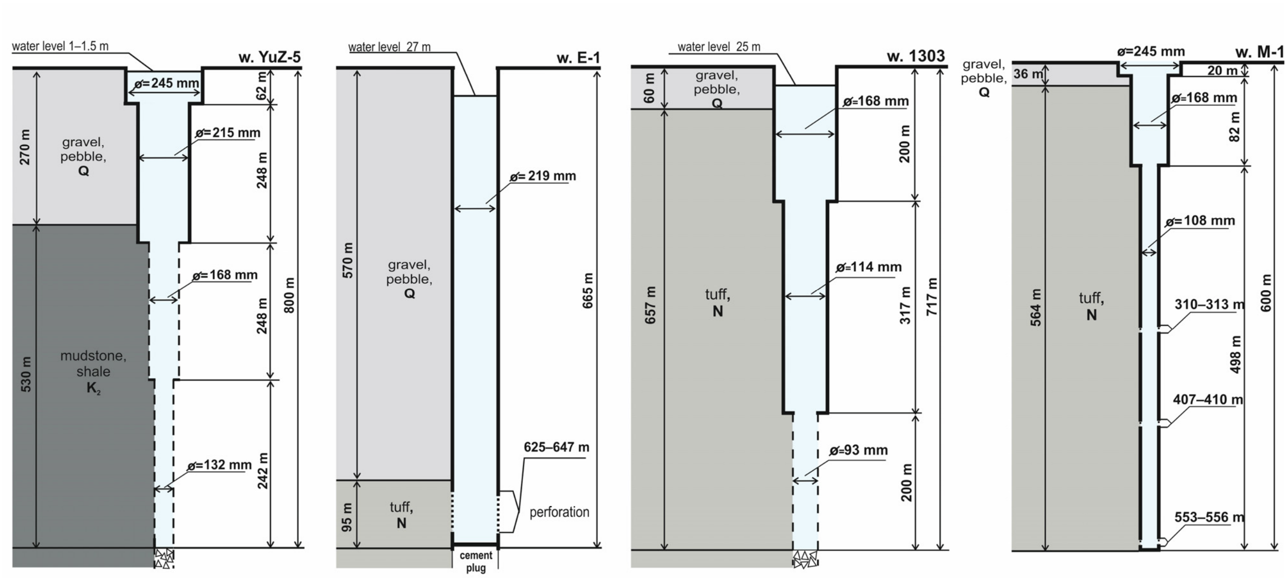

Figure 2. Wells' structure and geological section.

The wells open up pressure aquifers in the areas of casing perforation at depths of 310–1100 m. The exposed water-bearing rocks consist of tuffaceous–sedimentary rocks of Neogene age and terrigenous metamorphosed deposits of Late Cretaceous age with predominantly fracture permeability. These aquifers are characterized by static confined conditions [13–16]. For such conditions, when opening an aquifer with a piezometric well, a direct relationship is observed between changes in water pressure and deformation of water-bearing rocks controlled mostly by the aquifer elastic parameters.

Analysis of the relationship between the water level changes with atmospheric pressure and theoretical earth tide variations showed distinct barometric and tidal responses in the piezometric wells YuZ-5 and 1303 in the range of hourly and daily periods, while there was a weak barometric response and no tidal response of groundwater pressure in self-flowing well M-1. We believe that this is caused by the dissipation of barometric and tidal signals in water pressure changes at the perforation depths of the wellbore by the free flow of water from well M-1. At the same time, the depth opening of water-bearing rocks of 310–556 m (Figure 2), the constancy of water pressure and discharge, as well as the stability in chemical composition of underground water throughout the year, allow us to accept static confined conditions for well M-1.

In water level changes in well E-1, a weak barometric response was detected in the range of periods of two or more days, as well as the absence of a tidal response in the range of diurnal and semidiurnal tidal waves. We believe that such features of this well are associated with the increased compressibility of underground water containing methane–nitrogen gas (Table 1).

The results of barometric and tidal analysis of water level variations in piezometric wells indicate the presence of statically confined conditions and allow us to estimate the elastic properties of aquifers (Table 3). The values of Skempton's coefficient B and specific elastic capacity S_s of water-bearing rocks, as well as porosity ϕ, were obtained by calculation using the values of barometric efficiency E_b and tidal sensitivity A_v according to [17,18]. The values of the filtration parameters—transmissivity T and hydraulic conductivity—were obtained from well tests after the completion of drilling.

Table 3. Elastic and filtration properties of water-bearing rocks [5,13].

Wells	Barometric Efficiency, E_b,	Tidal Sensitivity, A_v*, hPa/10^{-9}	Skempton's Coefficient, B	Specific Elastic Capacity, S_S, $m^{-1} \times 10^{-7}$	Porosity, ϕ	Transmissivity, T, m^2/Day	Hydraulic Conductivity, m/c
YuZ-5	0.40	0.161	0.67	16.9	0.11	7.8	9×10^{-7}
E-1	0.1	–	0.09	2.9	0.05	0.005	3.2×10^{-9}
1303	0.43	0.215	0.64	10.3	0.07	0.32	3.7×10^{-8}

Notes: * A_v is tidal sensitivity of water pressure with respect to the theoretical volumetric strain.

The duration of continuous observations of water level/pressure variations using digital equipment in individual wells varies from 28 to approximately 3 years (Table 1). The description of the equipment is given in [4,5]. During the EQ, as well as throughout the entire period of precision observations, all wells were equipped with precision sensors for groundwater pressure/level and atmospheric pressure, providing an accuracy of ±0.1 hPa.

The study of seismo-hydrogeodynamic effects in the groundwater pressure changes in Kamchatka wells has shown that they can manifest themselves in a wide range of periods—from seconds to hours and days to tens of days. This diversity in the manifestations of SHGE over time is consistent with observations in other regions during strong earthquakes [1,2,19–25].

It should be noted that the detail of the SHGE study, especially high-frequency variations in water pressure due to the passage of seismic waves, is determined by the frequency of pressure/level measurements in observation wells. With hourly measurements, it is not possible to study high-frequency variations in groundwater pressure. With measurements in the range of minutes, we can only state the fact of high-frequency variations in water pressure during the passage of seismic waves from strong earthquakes, but it is impossible to consider them in detail with accurate estimates of amplitudes and frequency content [26,27].

When conducting observations with a frequency ≥1 Hz, for example, [24], records of water pressure fluctuations and subsequent post-seismic changes can be obtained, the features of which are explained by the occurrence of a complex of hydrogeodynamic processes in the well–aquifer system, determined by local natural conditions, as well as differences in the structure of wells. This is consistent with the authors' opinion [26], as well as the opinion of the authors of [28], that each observation well is a unique object for recording and subsequent study of seismo-hydrogeodynamic effects both in the high-frequency domain with periods of seconds to minutes and in the low-frequency hourly to daily range.

For the convenience of describing the individual types of SHGEs in Kamchatka wells, their entire set was divided into:

(i) "high-frequency effects" in groundwater pressure changes caused by the vibration impact of seismic waves and change in the static stress state of water-bearing rocks, as well as short-term disruption of quasi-stationary filtration of underground water near the wellbore, lasting from minutes to hours;
(ii) "low-frequency effects" in groundwater pressure changes during the preparation of earthquakes and relaxation of the disturbed state of the well–aquifer system at the post-seismic stages, lasting for a day or tens of days.

The identification of "high-frequency effects" was carried out using fragments of the initial level/pressure records with a minimum frequency of measurements, including the arrival time of seismic waves at the nearest PET seismic station (Figure 1). In 1996–2018, such minimum recording frequency at wells YuZ-5 and E-1 was 5–10 min. Starting from 2017–2020, after the modernization of equipment at all four wells [4], the minimum frequency of observations is 1 Hz in wells YuZ-5, 1303, M1. At well E-1, water level measurements were taken every 5 min and water pressure was measured at a depth of 6 m below the water level every 2 min. Atmospheric pressure is measured at a frequency of 5 min directly at all wells.

The identification of "low-frequency effects" in water pressure changes was carried out using time series of hourly average data obtained by averaging the initial level/pressure records in a time window of 1 h. In the obtained hourly average data series of water level/pressure recording, adaptive compensation for tidal and barometric variations based on an estimate of the complex transfer function from atmospheric pressure variations to water level changes was carried out in accordance with the algorithm described in [5,29].

The identification of anomalies in the water level/pressure change in well E-1 was carried out using daily time series after compensation for barometric variations.

For well YuZ-5, based on long-term observations, an average seasonal head change function was constructed with a data sampling frequency of 1 day [5], which was used to diagnose the seismo-hydrogeodynamic effects lasting tens of days. Such long-lasting SHGEs were distinguished by a significant deviation of the current values of groundwater pressure from the behavior of the average seasonal head function. The deviations in current water level/pressure values of at least ±10 cm in relation to the seasonal average pressure function for about a month or more were taken as an anomaly.

A mandatory element of data processing for identifying the SHGE is monitoring the influence of the loading effect from atmospheric precipitation. For this purpose, observation data of daily precipitation amounts at the nearest weather station Pionerskaya are used (Figure 1b). It has been empirically established that with precipitation of more than 15–20 mm/day, an increase in water pressure with amplitude of 1–2 hPa may occur during the 1–2 days. Besides this, prolonged increases in water pressure in the YuZ-5 well sometimes occurred after abnormal amounts of precipitation (up to 75–150 mm/day) during autumn cyclones [5]. Such meteorological phenomena can be accompanied by significant deviations in the intra-annual seasonal change in water pressure compared to the behavior of the long-term average seasonal pressure function.

3. Characteristics of Previously Observed SHGE

The long-term time series of observations were obtained for wells YuZ-5 and E-1 (Table 1). During such long time intervals, numerous earthquakes occurred in a wide range of magnitudes at different epicentral distances to the wells. These earthquakes were accompanied by seismo-hydrogeodynamic effects that differed in morphology and duration, as well as in time relative to the earthquake moments. The presence of multiple earthquakes and corresponding SHGEs allow us to generalize such data for individual wells showing the dependence of SHGEs' various morphologies and durations on the earthquake parameters—the ratio of their magnitudes and epicentral distances, density of seismic energy in the wave in the well area [30] and the ratio between epicentral distances of the well and linear size of the earthquake sources [31]. An example of a graphical representation of the typification of seismo-hydrogeodynamic effects for well YuZ-5 is given in the work ([5], Figure 14).

Below, in Sections 3.1–3.3, a brief description of the SHGEs recorded in observation wells during the previous observation period is presented.

3.1. Well E-1: Typification of Seismo-Hydrogeodynamic Effects

Well E-1 opens up brackish groundwater in Neogene tuffs in the depth range of 625–648 m (Figures 1, 2 and Table 1) in a hydrodynamic zone of weak water exchange. Such conditions are indicated by the absence of annual seasonality in water level changes, as well as increased mineralization of underground water and the methane–nitrogen composition of the dissolved gas.

In well E-1, the total duration of water level/pressure observations is more than 37 years. In 1987–1995, observations were made using mechanical water level recorders. Digital measurements have been carried out since January 1996 to the present day. In well E-1, experiments on geothermal measurements with periodic disturbances of the hydrogeodynamic regime were carried out from 1999 to September 2002. Therefore, these data, as well as other relatively short breaks in observations, were excluded from consideration when studying the SHGE. Since 2020, a set of equipment has been operating at well E-1 to measure the water level and atmospheric pressure with a frequency of 5 min, as well as a set of equipment to measure the pressure, temperature and electrical conductivity of water at depth of 6 m below the water level with a frequency of once every 2 min [4].

In well E-1, a characteristic feature of water level changes is the increases and decreases lasting 3–6 years with amplitudes from the first tens of cm to 1.5 m with an average rate of ≤0.1 cm/day. Against the backdrop of such trends, weak barometric variations in water levels and changes associated with strong earthquakes appear [13]. The SHGEs registered in this well are presented in [3,31] and include:

(i) hydrogeodynamic precursors in the form of a decrease in water level at an increased rate before local earthquakes with M_w = 5.0–8.3;
(ii) post-seismic increases in water level after earthquakes with M_w = 6.0–8.3.

Epicentral distances of local earthquakes accompanied by manifestations of hydrogeodynamic precursors and post-seismic increases in water level are d_e = 70–360 km.

3.1.1. Statistical Significance of Hydrogeodynamic Precursor for Earthquake Prediction

The works in [3,13,31] describe in detail the hydrogeodynamic precursor (HGP), which manifests itself in an increase in the daily rate of decrease in water level/pressure during the days to weeks before earthquakes with $M_w \geq 5.0$ at epicentral distances of up to 360 km. Figure 3 shows a schematic diagram of the diurnal rate of water level variations during the HGP. The threshold value of the daily rate of water level decrease at which the precursor was identified was determined empirically based on observations in 1987–1995 and it was confirmed by later digital observations.

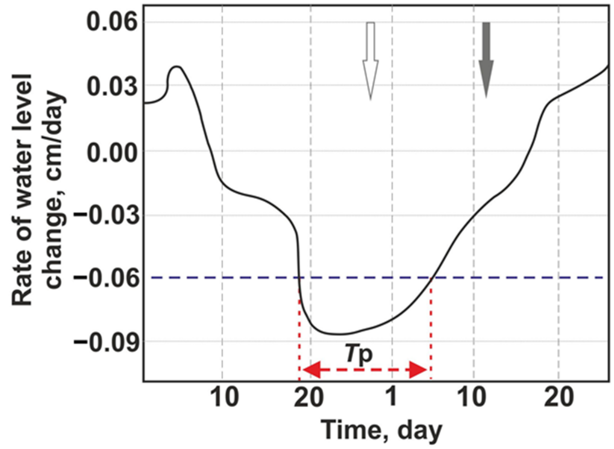

Figure 3. Scheme of hydrogeodynamic precursor in water level changes in well E-1. The horizontal dotted line is the threshold value of the water level decrease rate, determined empirically. *T*p—time of precursor manifestation. The vertical arrows show possible times of earthquake occurrence: unfilled arrow—earthquakes occur in approximately 10% of cases, filled arrow—earthquakes occur in approximately 90% of cases [3].

Table 4 presents the retrospective assessment of the seismic forecasting effectiveness using the hydrogeodynamic precursor (HGP) based on precision observations from February 1996 to 2023, a total of 22.16 years, taking into account technical gaps in the observations. Two assessment options are presented: (i) for earthquakes with $M_w \geq 5.0$ and (ii) for earthquakes with $M_w \geq 5.8$ that occurred within a radius of up to 360 km from well E-1. Previously, in ([3], Supplementary Material, Table S3), similar statistical estimates were presented for the time interval from February 1996 to October 2012.

Table 4. Retrospective assessment of the parameters of the effectiveness of using a hydrogeodynamic precursor in the water level changes in well E-1 for seismic forecasting over the observation period from February 1996 to December 2023.

Data for analysis	Water level observation data from well E-1 (53.26° N, 158.48° E), February 1996 to December 2023, total time of continuous observations T = 8090 days (22.16 years)
Earthquake monitoring area	A region within a radius of 360 km from well E-1
Studied parameter	Daily rate of water level changes with corrected for barometric variations and trend
Precursor signal HGP	Increasing the daily rate of water level decline to ≤−0.06 cm/day for at least 5 days
Retrospective analysis of HGP for forecasting the earthquakes with $M_w \geq 5.0$	
Total number of earthquakes, n	109
Total number of HGP manifestations before earthquakes (successful forecasts), m	49
Probability of correlation between HGP manifestations and earthquakes, P = m/n	P = 49/109 = 0.45
Probability of missing a target, $P_{mt} = (n - m)/n$	$P_{mt} = (109 - 49)/109 = 0.55$
Total number of HGP manifestations, m′	62

Total number of cases when no earthquake occurred after HGP manifestations (false alarms)	13
Probability of a successful forecasts for HGP manifestations, $P' = m/m'$	$P' = 49/62 = 0.79$
Probability of false alarm, $P_{fa} = (m' - m)/m'$	$P_{fa} = (62 - 49)/62 = 0.21$
Total alarm time, τ	2365 days
Ratio of total alarm time to total observation time, τ/T	2365/8090 = 0.29
Efficiency of HGP for forecasting the earthquakes with magnitude $M_w \geq 5.0$, $J = P/(\tau/T)$	$J = 0.45/0.29 = 1.55$
Retrospective analysis of HGP for forecasting earthquakes with $M_w \geq 5.8$	
Total number of earthquakes, n	31
Total number of HGP manifestations before earthquakes (successful forecasts), m	21
Probability of correlation between HGP manifestations and earthquakes, $P = m/n$	$P = 21/31 = 0.68$
Probability of missing a target, $P_{mt} = (n - m)/n$	$P_{mt} = (31 - 21)/31 = 0.32$
Probability of a successful forecast for HGP manifestations, $P' = m/m'$	$P' = 21/62 = 0.34$
Probability of false alarm, $P_{fa} = (m' - m)/m'$	$P_{fa} = (62 - 21)/62 = 0.66$
Efficiency of HGP for forecasting the earthquakes with magnitude $M_w \geq 5.8$, $J = P/(\tau/T)$	$J = 0.68/0.29 = 2.34$

A retrospective parametric description of the HGP includes an assessment of five statistical quantities characterizing the features of the relation between the forecasts based on this kind of precursor and subsequent earthquakes of a given energy range in a given spatial area ([3], Supplementary Materials, Explanation to Table S3):

1—probability of a connection between successful forecasts of earthquakes according to HGP and earthquakes, equal to the ratio of successful forecasts to the total number of earthquakes that have occurred (P);

2—probability of missing a target, equal to the ratio of the number of not predicted earthquakes to the total number of earthquakes that occurred (P_{mt});

3—probability of successful forecasts of earthquakes during occurrence of HGP, equal to the ratio of the number of HGP manifestations before earthquakes to the total number of HGP manifestations (P′);

4—probability of false alarm, equal to the ratio of the number of HGP manifestations, after which no earthquake occurred, to the total number of HGP manifestations (P_{fa});

5—retrospective efficiency of earthquake forecasts on base of HGP (J).

We used the approach in [32] to assess the retrospective efficiency of earthquake forecasts on the basis of HGP. If the forecast according to the specified technique is given for the same spatial area (within a radius of up to 360 km from well E-1) and for the same energy range of earthquakes ($M_w \geq 5.0$ and $M_w \geq 5.8$), then the efficiency of this technique J can be estimated by the formula:

$$J = (m/n)/(\tau/T) = P/(\tau/T), \quad (1)$$

where m is the number of "predicted" earthquakes, that is, those that correspond to successful forecasts; n is the total number of earthquakes that occurred with parameters (location–energy) that correspond to the forecast, that is, earthquakes that could be predicted; τ is total alarm time, that is, the total duration of all successful and unsuccessful forecasts, including the time of all cases of HGP manifestation up to the moment of the earthquake minus the first 5 days of the HGP manifestation in each case of HGP manifestation or, in the case of "false alarms", the durations of HGP minus 5 days and plus 30 days corresponding to the waiting time of the earthquake after the end of the HGP manifestation (Figure 3) and T is the total time of monitoring the seismic situation by the technique that is being assessed.

Accordingly, the efficiency J is the ratio between the number of predicted earthquakes according to HGP and the number of those events that could occur accidentally during an alarm time, assessed by the ratio of τ/T. Obviously, the random guess method would make the value J equal to 1. If the value J > 1, then this technique is useful for predicting earthquakes.

During the entire period of digital observations at well E-1 over 22.16 years, 109 seismic events with magnitudes $M_w \geq 5.0$ within a radius of up to 360 km were considered. In the case of several earthquakes with a magnitude of $M_w \geq 5.0$ that occurred within a time interval of up to one month at a distance of up to 360 km from the well, only the event with the maximum magnitude was considered. There were 25 of 109 such events (22.9%), corresponding either to the aftershocks following the strong earthquake or to an earthquake swarm. In all such cases, the choice of the event to be taken into account was made from a number of earthquakes from 2 to 31.

It was believed that after the end of precursor manifestation, the waiting time for an earthquake could be no more than 30 days. That is, the alarm time formally included the time of precursor manifestation minus 5 days plus the time up to 30 days from the end of earthquake precursor. If, during the time up to 30 days after the end of precursor, the earthquake does not occur, then in this case, the precursor manifestation was considered a false alarm and was included in the general alarm time τ.

To test the stability of statistical parameters of the predictive efficiency of the HGP, we also calculated the statistical parameters of the seismic forecasting efficiency of hydrogeodynamic precursor for the time interval December 2012–December 2023. Below, we present the refined estimates of statistics for three observation periods: (February 1996–October 2012):(December 2012–December 2023):(February 1996–December 2023) when predicting earthquakes with $M_w \geq 5.0$:

T, days = 4042:4048:8090;
n = 58:51:109;
m = 26:23:49;
P = m/n = 0.45:0.45:0.45;
P_{mt} = (n − m)/n = 0.55:0.55:0.55;
m′ = 32:30:62;
Total number of false alarms = 6:7:13;
P′ = m/m′ = 0.81:0.76:0.79;
P_{fa} = (m′ − m)/m′ = 0.19:0.23:0.21;
Time of alarm τ, days = 1316:1049:2365;
τ/T = 0.33:0.26:0.29;
J = P/(τ/T) = 1.36:1.73:1.55.
In case of retrospective forecasting of earthquakes with $M_w \geq 5.8$:
n = 13:18:31;
m = 11:10:21;
P = m/n = 0.85:0.56:0.68;

P_{mt} = 0.15:0.44:0.32;
P′ = 0.34:0.33:0.34;
P_{fa} = 0.66:0.67:0.66;
J = 2.58:2.15:2.34.

As can be seen from the given parameters of retrospective forecasting of earthquakes based on the HGP, its statistical significance is relatively small, $J_{Mw\geq5.0}$ = 1.55 and $J_{Mw\geq5.8}$ = 2.34. At the same time, the obtained estimates of value J > 1 show that the use of a precursor is useful in predicting earthquakes, since it exceeds their random guessing. Besides this, the parameters of statistical significance of the precursor for predicting earthquakes with $M_w \geq 5.0$ and $M_w \geq 5.8$, estimated for time intervals from 10 to 22 years, remained quite stable.

Thus, the estimates of predictive statistical significance of the precursor in water level change made it possible to use this precursor for the current forecasting based on observation data from well E-1 together with other seismic forecast data.

3.1.2. Post-Seismic Increases in Water Pressure

In well E-1, smooth post-seismic increases in the water level with amplitudes from 2 to 30 cm over a period of 1–3 months were recorded after ten earthquakes with magnitudes of 6.0–8.3 at epicentral distances of 70–350 km ([3] (Supplementary Materials), [13,31,33]). These were the strongest earthquakes, and they were accompanied by noticeable tremors with an intensity of 4 to 6 points on the macroseismic 12-point intensity scale *MSK*-64 [34].

We believe the post-seismic increases in water level after strong earthquakes could have been caused by the influx of water into the wellbore from water-bearing rocks, as well as due to a decrease in the density of water in the wellbore with increase in the proportion of free methane–nitrogen gas in water in the wellbore as well as in surrounding water-bearing rocks, caused by intense seismic shaking.

Similar gradual increases in water level after strong earthquakes were recorded in the BV well in California [18]. For this well, the influence of transitions of dissolved gas into a free state is also assumed during post-seismic rises in water level. Unfortunately, data on the composition of the gas are not provided.

3.2. Well YuZ-5: Seismo-Hydrogeodynamic Effects and Their Typification

In well YuZ-5 (Figure 2; Table 1), water level/pressure observations have been carried out since September 1997 (27 years). The results of observations, including a description of various types of seismo-hydrogeodynamic effects, are presented in detail in [5].

In this well, three types of SHGEs were identified:

(i) supposed hydrogeodynamic precursors before the two strongest earthquakes, manifested in a violation of the seasonal change in hydrostatic head during the first tens of days;
(ii) coseismic jumps in water pressure within minutes (1–12 min) due to changes in the static stress state of water-bearing rocks during the rupturing in the sources of local earthquakes;
(iii) four (I–IV) types of vibration effects of seismic waves in water pressure changes lasting from minutes to tens of days, the morphological features of which are determined by the amplitude–frequency composition of seismic waves from earthquakes recorded at the nearest PET seismic station [26].

3.2.1. Supposed Hydrogeodynamic Precursors

Previously, the supposed hydrogeodynamic precursors were identified by a significant deviation of the water pressure values from the average long-term head pressure function in well YuZ-5 before the Kronotsky (KE) earthquake on 5 December 1997, M_w = 7.8 and before the Zhupanovsky earthquake (ZhE) on 30 January 2016, M_w = 7.2 [5,31].

In the case of KE, the preceding excessive decrease in water pressure was Δh = 11 cm of the water column for ≈20 days. Before the ZhE, the excess of water pressure relative to its seasonal position was approximately Δh = 30 cm over 90 days with an average standard error of seasonal trend determination of ±10.4 cm of the water column [5]. Unlike well E-1, in which the precursor appears uniformly before all the earthquakes under consideration, in well YuZ-5, the supposed precursors appeared both in an excessive decrease (the case of KE) and in an increase in the level/pressure of underground water (the case of ZhE). This allows us to assume the action of the mechanism of quasi-elastic deformation of water-bearing rocks near well YuZ-5, which occurs due to aseismic movements in the area of earthquake sources preceding the main events.

Based on the assumption that the leading mechanism of water pressure change is due to quasi-elastic deformation of water-bearing rocks near the wellbore, the amplitudes of volumetric deformation before KE were estimated: $D_{(KE)} = \Delta h/A_v$ = 11 cm/0.161 cm/10^{-9} = 68 × 10^{-9} ≈ 0.7 × 10^{-7} (expansion) and before ZhE $D_{(ZhE)}$ = −30 cm/0.161 cm/10^{-9} = −186.3 × 10^{-9} ≈ −1.9 × 10^{-7} (compression), where A_v is the tidal sensitivity of the water level in well YuZ-5 (Table 3). The given values of volumetric deformations of water-bearing rocks in the area of well YuZ-5 during the preparation of two strong earthquakes are hypothetical and approximate due to the evaluative nature of the quasi-elastic response of water pressure in the well.

3.2.2. Coseismic Effects in Water Pressure Changes

In well YuZ-5, coseismic jumps of water pressure were recorded, caused by a change in the static stress state of water-bearing rocks during the formation of rupture in the earthquake sources (coseismic effects—CSEs). Examples and descriptions of coseismic effects are given in the works of the authors [5,27]. Such effects developed during the time from the first minutes to 12 min after the arrival of seismic waves. The amplitudes of coseismic jumps in water pressure were 0.2–12 cm of the water column.

Previously, in the mentioned works, it was convincingly shown that the amplitudes and direction of coseismic changes in water pressure in well YuZ-5 are in satisfactory agreement with theoretical estimates of coseismic deformation in the well area (D_2) in accordance with the dislocation model [35] with the parameters of earthquake focal mechanisms.

The values of coseismic deformation in the well area (D_1) were also determined based on the amplitudes of water level/pressure changes Δh_{CSE}, with use of the value of tidal sensitivity A_v (Table 3) as a coefficient normalizing the amplitudes of coseismic jumps in water level:

$$D_1 = -\Delta h/A_v, \quad (2)$$

where D_1 is the volumetric coseismic deformation in units of 10^{-9}, and Δh is the amplitude of coseismic water level change in cm. The sign of deformation was assessed by the directions of water level/pressure change: volumetric compression of water-bearing rocks with an increase and volumetric expansion with a decrease in water level/pressure. In work ([5], see Table 3; Figures 10 and 11), the values D_1, calculated for 14 earthquakes, are compared with the theoretical estimates of coseismic strain D_2 according to the dislocation model [35] with parameters of earthquake sources for the observation period from 1997 to 2020. It was established that coseismic pressure jumps in well YuZ-5 occur during earthquakes described by the equation $M_w \geq 0.004 \times d_e + 5.0$. In fact, the parameters of such earthquakes were M_w = 5.4–8.3, and the epicentral distances of such earthquakes to the well were d_e = 86–700 km.

3.2.3. Vibration Effects of Seismic Waves

A meaningful description of four types of vibration effects of seismic waves from strong earthquakes with M_w = 6.9–9.1, occurring at epicentral distances of d_e = 80–14,600 km, is given in [26], and also in ([5], see Section 3.4).

Table 5 provides a brief description of the identified morphological types of seismo-hydrogeodynamic effects in water level changes with amplitudes of ≥0.4 cm that occur under the influence of seismic waves, taking into account the parameters of earthquakes M_w, d_e and the value of the specific density of seismic energy in the wave e. The e values were estimated by the following formula [30]:

$$\log d_e = 0.48 \times M_w - 0.33 \times \log e - 1.4. \quad (3)$$

The amplitudes and frequency ranges of the maximum phases of ground motions were estimated from three-component broadband earthquake records by the STS-1 sensor at the PET seismic station (Figure 1) [26].

Table 5. Vibration effects of seismic waves in water level changes in well YuZ-5 [5,26].

Type	Morphology and Duration	M_w	d_e, km	e, J/m³	Proposed Mechanism
I	Forced and free oscillations of water level during the time from hours to about one day with amplitudes 0.4–2 cm	7.8–8.7	6800–14,600	10^{-3}–10^{-4}	The impact of surface waves with periods of at least tens of seconds during the strong distant earthquakes, accompanied by a resonant effect of amplification of water pressure variations in the well–aquifer system [36]
II	Water level oscillations with superimposed short term, from minutes and hours to days, residual rises with amplitudes 1–7 cm	8.2–9.1	810–8260	10^{-1}–10^{-3}	Impact of surface seismic waves with superposition of short-term (minutes) pulse of increase in water pressure and nonlinear filtration of groundwater near the wellbore
III	Residual water level rises lasting for hours to first day with amplitudes 1–9 cm	7.6–8.3	720–5170	10^{-1}–10^{-4}	Short-term increase in water pressure and nonlinear filtration near the wellbore
IV	Long-term (1.5–3 months) water level lowering with amplitudes 0.28–1.0 m	6.9–7.8	86–260	1–10^{-2}	Water pressure drop in the aquifer at a distance of up to 450 m from a well due to a change in the permeability of water-bearing rocks under the impact of high-frequency body seismic waves and tremors of 5–6 points *MSK*-64

A clear dependence of the identified four (I–IV) types of vibration effects on the intensity of seismic impact in the well area (the ratio of magnitude M_w and distance of earthquakes d_e, value e, macroseismic intensity) and the amplitude–frequency composition of seismic waves was established. Low-frequency and low-amplitude surface waves from distant earthquakes were accompanied by water level oscillations (type I). With the increase in the amplitude of the seismic signal, short-term water level increases were superimposed on oscillations (type II). Relatively high-frequency signals of surface waves were accompanied by short-term water level rises (type III). In the cases of the strongest local earthquakes accompanied by the passage of intense body waves and perceptible shaking with the intensity of I_{MSK-64} = 5–6 points, the decreases in the water level occurred over 1–3 months (type IV) ([5], see Figure 13).

3.3. Seismo-Hydrogeodynamic Effects in Wells 1303 and M-1

Since 1984, the KB GS RAS has been conducting observations on the discharge rate, temperature and chemical composition of underground water at self-flowing well M-1 with a frequency of 3−6 days [3]. In this well, abnormal changes in the chemical composition of water were recorded, including hydrogeochemical precursors to strong earthquakes with M_w = 6.5–7.5, which occurred at epicentral distances of 100−230 km [3,37].

At well 1303, since the beginning of the 21st century, observations have been carried out on changes in the water level using mechanical float recorders and digital equipment by organizations of the Ministry of Natural Resources of the Russian Federation. The frequency of water level and atmospheric pressure measurements was 1 h. According to 10 min measurements, a post-seismic rise in the water level was recorded after the Olyutor earthquake of 20 April 2006, M_w = 7.6 in the north of Kamchatka, which occurred at a distance of 1040 from the well. The amplitude of water level rise was 0.35 cm within 30 min.

The precision observations of pressure variations in wells M-1 and 1303 are relatively short and amount to 3.6 and 2.8 years (Table 1).

In well M-1, according to precision observation with a frequency of 1 Hz from 2020 to 2024, water pressure fluctuations with amplitudes of 0.1−0.2 hPa for 10−20 min during the passage of surface seismic waves from five strong distant earthquakes (M_w = 7.4−8.2, d_e = 2600−9800 km), occurring in Alaska, Turkey, Japan and Taiwan, were recorded.

After installing precision equipment in well 1303 for recording water pressure with a frequency of 1 Hz, the pressure fluctuations with maximum amplitudes of 0.1−0.3 hPa were recorded during the passage of surface seismic waves from six strong (M_w = 7.4−8.2) distant (d_e = 4500−9800 km) earthquakes in Alaska, Japan, Turkey, the New Hebrides Islands and Taiwan. The duration of such pressure fluctuations was 10−40 min.

The recorded vibration seismo-hydrogeodynamic effects in wells 1303 and M-1 during strong distant earthquakes approximately correspond to type I SHGEs in well YuZ-5 (Table 5).

4. Seismo-Hydrogeodynamic Effects of the 3 April 2023 Earthquake

4.1. 3 April 2023 Earthquake, M_w = 6.6

The earthquake of 3 April 2023 (hereinafter EQ) (Figure 1a; Table 2) was one of the strongest seismic events in the Petropavlovsk–Kamchatsky test site area during the period of precision observations in wells. The wells are located at epicentral distance d_e = 67–77 km (hypocentral distance d_h = 116–122 km). The maximum linear size of the earthquake source is L = 41.2 km (Table 2) and approximately corresponds to the length of the aftershock activation area during the first day (Figure 1a). The ratio between the epicentral distance to the observation wells and the size of the earthquake source is d_e/L = 1.6_{YuZ-5} − 1.9_{E-1}. In the wells' area, the macroseismic intensity of shaking was 6 points on the 12-point *MSK*-64 scale [34].

At the PET seismic station, located at a distance of 23–30 km from the wells (Figure 1), the arrival of body P–wave was recorded at 03:07:12, S–wave at 03:07:24 (Figure 4). Surface waves were not detected in the seismic record of the EQ in PET station due to the close location of the earthquake's source.

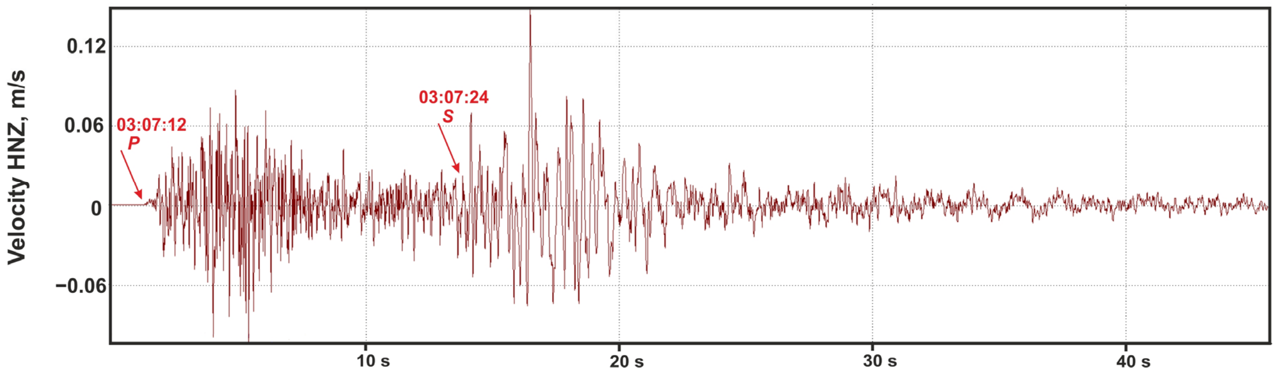

Figure 4. Seismic recording on the HNZ channel in PET seismic station (53.023° N, 158.65° E), 100 Hz. P, S—seismic waves.

Figure 5 shows the distribution of coseismic volumetric strain during EQ at a depth of 500 m, corresponding to the average depth of the open part of the wellbores of wells YuZ-5 and 1303. In the area of the wells, the expansion calculated value of water-bearing rocks was 2.3×10^{-8}.

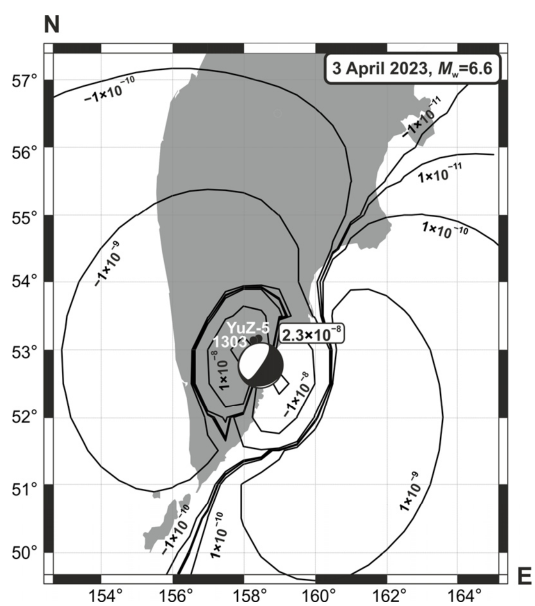

Figure 5. Distribution of coseismic volumetric strain at depth of 500 m calculated from the dislocation model [35] and data on the earthquake source mechanism (Table 2), indicating the D_2 value (volumetric expansion 2.3×10^{-8}) in the area of wells YuZ-5 and 1303 (the wells are shown by the black circles). The values of compression strain correspond to the sign "−", and expansion strain to the sign "+".

4.2. Seismo-Hydrogeodynamic Effects

4.2.1. SHGE in High-Frequency Records of Water Pressure Variations

Figure 6a shows the records of water pressure with a frequency of 1 Hz in wells YuZ-5, 1303 and M-1 for five hours, including the moment of the EQ. Figure 6b shows the pressure variations in more detail over two minutes in comparison with the seismic record on the vertical channel of the PET seismic station.

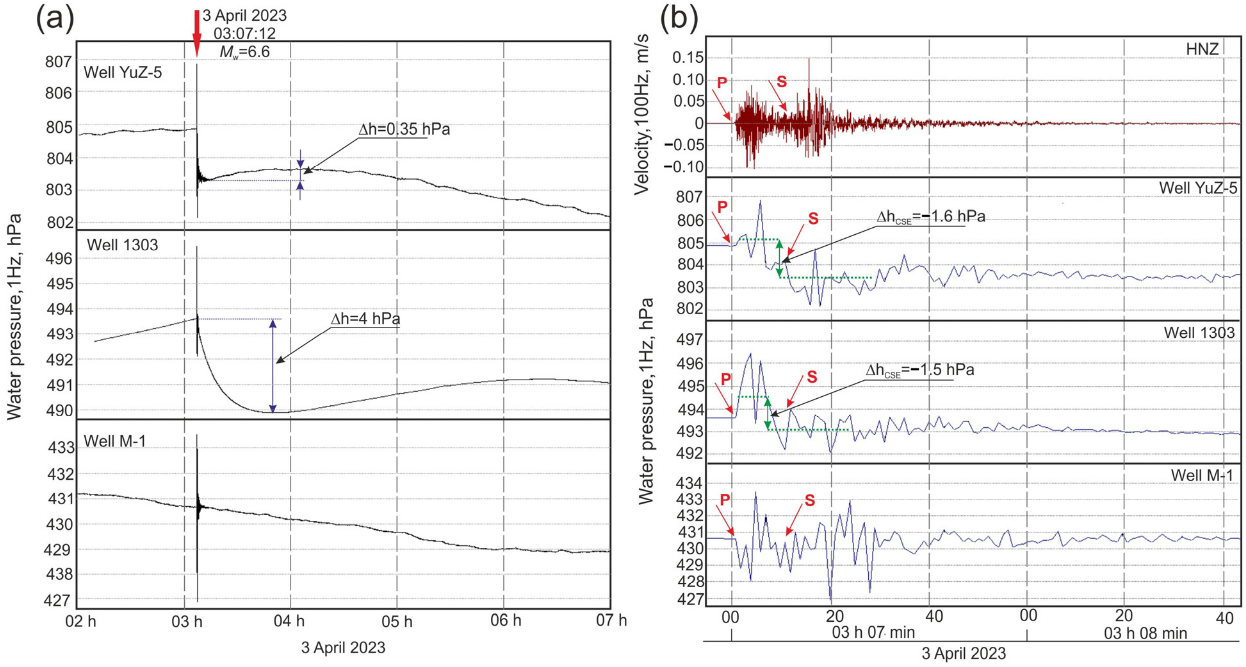

Figure 6. Water pressure variations with a frequency of 1 Hz in wells YuZ-5, 1303 and M-1 caused by the 3 April 2023 earthquake. (**a**) Over 5 h, including the moment of the earthquake (shown by the red arrow). (**b**) Within 2 min after the arrival of seismic waves at the PET station in comparison with the record on the HNZ channel (upper panel): arrival of P−longitudinal waves in 03:07:12, arrival of S−transverse waves in 03:07:24.

High-frequency variations in water pressure were recorded in all of these wells, which occurred during the arrival of body P and S waves. The maximum amplitudes of such variations were 3–4 hPa in the piezometric wells YuZ-5 and 1303. In the flowing well M-1, the amplitude of pressure variations was 6 hPa. Such high-frequency water pressure oscillations were caused predominantly by vertical displacements of the wellbores during the passage of seismic body waves [36].

In the records in wells YuZ-5 and 1303, coseismic effects (CSEs) in the form of water pressure drops with amplitudes $\Delta h_{CSE} = -1.6$ hPa and $\Delta h_{CSE} = -1.5$ hPa (Figure 6b) were identified, which were estimated as the difference between average pressure values during the passage of P and S waves [5].

In the records of water pressure in well M-1 (Figure 6b, lower panel), the coseismic effect was not evident, apparently due to dissipation of the coseismic response of groundwater pressure in the aquifer by free flow of water in the wellbore.

The short-term post-seismic effects were recorded in water pressure changes in wells YuZ-5 and 1303 after the end of pressure fluctuations during the passage of seismic waves. In well YuZ-5, the increase in water pressure with amplitude of $\Delta h = 0.35$ hPa was recorded for 50 min (Figure 6a, upper panel). The most likely cause of this effect is the influx of water into the wellbore during short-term nonlinear filtration of underground water near the wellbore due to seismic waves. Previously, similar short-term increases in water pressure in this well have been observed during some strong earthquakes [5,33].

In well 1303, after the end of high-frequency pressure oscillations, a decrease in water pressure with amplitude of $\Delta h = 4$ hPa for forty minutes was observed (Figure 6a, middle panel). Such a relatively short-term post-seismic effect, as well as a coseismic pressure jump, were recorded in this well for the first time.

Also, for the first time, in 2 min records of pressure, temperature and electrical conductivity of water in well E-1, a decrease in pressure with amplitude of 12 hPa and an increase in electrical conductivity of water with amplitude of 9 μS/cm were detected during the time from 3 h 6 min to 3 h 10 min. An increase in water temperature of 0.01° C within 3 h was also recorded.

4.2.2. Coseismic Effects of EQ

The values of the coseismic deformation in the wells' area (D_1) were estimated on the amplitudes of water pressure changes Δh_{CSE} (Figure 6b) with the use of the values tidal sensitivity A_v as a coefficient normalizing the amplitudes of jumps in water pressure. The amplitudes of water pressure decreases during EQ correspond to the volumetric coseismic expansion in the area of wells YuZ-5 and 1303: $D_{1(YuZ\text{-}5)} = -\Delta h_{CSE(YuZ\text{-}5)}/A_{v(YuZ\text{-}5)} = 1 \times 10^{-8}$ and $D_{1(1303)} = -\Delta h_{CSE(1303)}/A_{v(1303)} = 0.7 \times 10^{-8}$, where A_v is the tidal sensitivity, 0.161 hPa/10^{-9} volumetric deformation in well YuZ-5 and 0.215 hPa/10^{-9} in well 1303 (Table 3).

The values $D_{1(1303)} = 0.7 \times 10^{-8}$ and $D_{1(YuZ\text{-}5)} = 1 \times 10^{-8}$ agree with each other and with the theoretical estimate of coseismic volumetric deformation in the wells' area $D_2 = 2.3 \times 10^{-8}$ (Figure 5) in sign (expansion) and in amplitude within the same order of magnitude.

Figure 7a,b show the distribution of 14 earthquakes ([5], see Table 3), which were accompanied by coseismic jumps in water level/pressure changes with amplitudes Δh_{CSE} $\geq$ 0.2 cm (hPa) in well YuZ-5, depending on magnitudes and epicentral distances of the earthquakes. Here, the red star shows the above data on EQ.

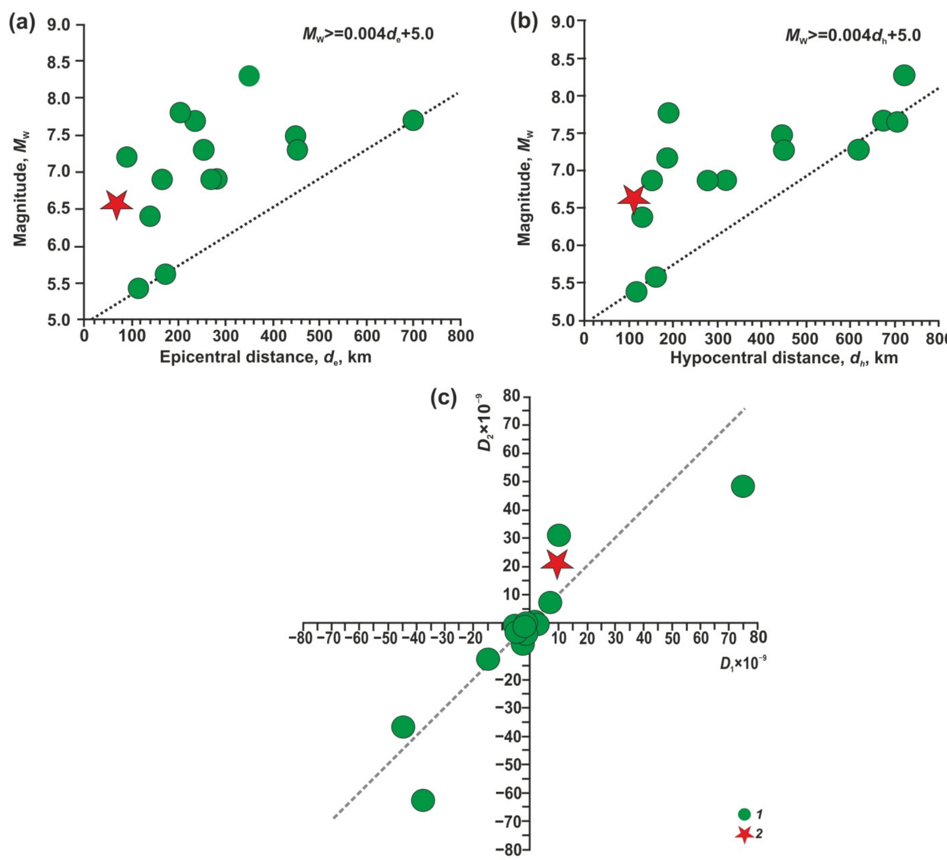

Figure 7. Distribution of 1997–2023 earthquakes, which were accompanied by coseismic jumps in water pressure in well YuZ-5 as a function of magnitude M_w and epicentral distance d_e (**a**) and hypocentral distance d_h (**b**). (**c**) Correlation between coseismic volumetric deformation in the YuZ-5 well area during local earthquakes obtained from observational data in the well (D_1) and from the dislocation model (D_2). 1—1997–2020 earthquakes (Table 3 in [5]), 2—3 April 2023 earthquake.

Despite the EQ occurring at the minimum epicentral distance from well YuZ-5 (Figure 7a), its coseismic manifestation corresponds to the general pattern of coseismic jumps in water pressure in this well depending on the earthquake parameters: $M_w \geq 0.004 \times d_e + 5.0$ and $M_w \geq 0.004 \times d_h + 5.0$ (here, d_e is the epicentral distance; d_h is the hypocentral distance in km).

The coseismic effects of EQ in well YuZ-5 approximately correspond to the parameters of coseismic effects during the earthquakes of 1 June 1998, $M_w = 6.4$ ($\Delta h_{CSE} = -1.0$ см, $D_1 = 0.6 \times 10^{-8}$, $D_2 = 0.6 \times 10^{-8}$) and 8 March 1999, $M_w = 6.9$ ($\Delta h_{CSE} = -1.7$ см, $D_1 = 1.1 \times 10^{-8}$, $D_2 = 3.1 \times 10^{-8}$) ([5], see Table 3)). These two earthquakes occurred relatively close to the EQ and had similar parameters of focal mechanism.

Figure 7c shows the distribution of values D_1 and D_2 for all 15 earthquakes accompanied by coseismic jumps with amplitudes of ≥0.2 cm (hPa). The values of coseismic deformation D_1 and D_2 obtained by the two methods are uniformly distributed with respect to the direct connection line. Such a distribution of the values of coseismic deformation indicates the absence of systematic errors in their determination using each of the methods. A consideration of possible errors in the estimates of coseismic deformation D_2 on the model of dislocation source and D_1 on the data of water level observations is given in [27].

4.2.3. SHGE in Average Hourly Variations of Water Pressure in Well YuZ-5

Figure 8 shows the water pressure changes in well YuZ-5 with compensated barometric and tidal variations in comparison with the behavior of annual seasonal function in hydrostatic head changes in the well area (shown by the grey line). The description of seasonal function construction is given in [5].

After the end of short-term co- and post-seismic variations in water pressure (see Section 4.2.1; Figure 6), a decrease in water pressure with amplitude of about 30 hPa was observed for two months (Figure 8b, upper panel). After subtracting the seasonal trend (2) from the recorded variations of water pressure with compensated barometric variations (1), the amplitude of post-seismic lowering in water pressure was rated as 24 hPa (Figure 8b, lower panel).

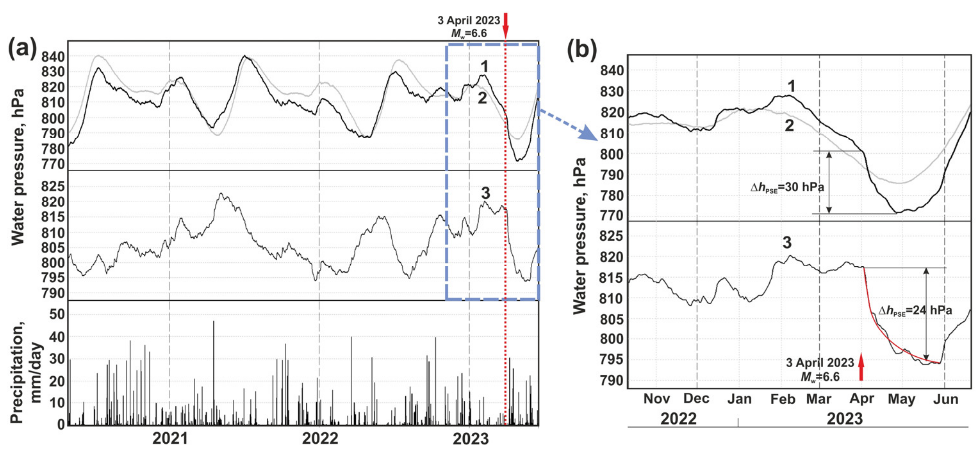

Figure 8. Average hourly water pressure variations in well YuZ-5 and atmospheric precipitation in May 2021–June 2023 (**a**): 1—average hourly pressure variations with compensated barometric variations (black line); 2—seasonal pressure variations (gray line); 3—residuals in water pressure changes after removal of annual seasonality; red arrow—earthquake on 3 April 2023, $M_w = 6.6$ (EQ). Bold dotted line denotes a fragment of pressure variations during EQ, shown in Figure (**b**). (**b**) Manifestation of the supposed hydrogeodynamic precursor and postseismic decrease in water pressure, corresponding to type IV vibration impact of seismic waves [26]; red line shows the calculated water level decrease according to Formula (4).

Previously, long-term postseismic decreases in water pressure were observed after three of the strongest seismic events: KE 5 December 1997, M_w = 7.8, d_e = 200 km; 28 February 2013, M_w = 6.9, d_e = 280 km and ZhE 30 January 2016, M_w = 7.2, d_e = 80 km. Such decreases in water level/pressure after earthquakes accompanied by a tremor with an intensity of 4–6 points on the *MSK*-64 scale were identified as type IV vibration effects of seismic waves (Table 5) [26].

The most probable mechanism for the post-seismic water level lowering in well YuZ-5 is a drop in head pressure in the aquifer due to a local increase in the permeability of water-bearing rock as a result of intense seismic shaking during the passage of body seismic waves [26,33].

The decrease in water level in a well can be described by Formula (4) [38], which represents the solution of the one-dimensional diffusion equation [39] for a remote source of head pressure drop in a homogeneous infinite aquifer:

$$x = x_0 - \Delta h \times \operatorname{erfc}\left(R/\sqrt{4 \times a \times t}\right), \quad (4)$$

where x is the water level in the well, x_0 is the initial water level in the well, $\Delta h = \Delta p/\rho g$ is the change in pressure head in the well when changing water pressure in the aquifer Δp, ρ is the density of water, g is the acceleration of gravity, R is the distance from the source of the pressure head drop to the well, a is the hydraulic diffusivity [40], t is the time.

The calculation according to (4) shows satisfactory agreement between the calculated function of water pressure decrease in the well (red line in Figure 8b, bottom panel) and the development of post-seismic pressure decrease after EQ at values of the amplitude of water pressure decrease Δh = 0.24 m, hydraulic diffusivity coefficient a = 0.25 m^2/s and distance to the source of head pressure drop in the aquifer R = 450 m.

The results of calculations of the water level drop according to (4) after strong earthquakes KE, 28 February 2013, ZhE and EQ, agree in determining the distance R to the source of head pressure drop. In all four cases, these values were the same, R = 450 m, for close values a = 0.25–0.22 m^2/s. This allows us to assume that at a distance of 450 m from well YuZ-5, there is an object whose permeability can increase sharply during seismic tremors with an intensity of ≥4–5 points on the *MSK*-64 scale. We believe that such an object is a zone of tectonic fracturing in the Late Cretaceous metamorphosed volcanogenic–sedimentary rocks, which controls the structure of the Avacha river valley and is covered by modern sedimentary deposits (Figure 1b). An increase in the permeability of such a zone during seismic shocks may be accompanied by decrease in groundwater pressure in the Late Cretaceous rocks in the well area.

Supposed Hydrogeodynamic Precursor

During the 2.5 months before the EQ, increased values of water pressure were recorded in well YuZ-5, exceeding the seasonal pressure by 10.2 hPa (Figure 8b, upper panel). During the period from November 2022 to March 2023, there were no abnormally high precipitation amounts (Figure 8a), which could cause an excessive increase in water pressure in well YuZ-5. The most noticeable increase in water pressure occurred from mid-January to mid-February 2023 (Figure 8b, bottom panel). We assume that such an excessive increase in groundwater pressure in relation to the average seasonal head pressure could be a manifestation of the hydrogeodynamic precursor of EQ.

Based on the assumption of a quasi-elastic mechanism for this precursor, the volumetric deformation during the preparation of EQ can be estimated as $D_{(EQ)}$ = −10.2 cm/0.161 cm/10^{-9} = −63.4 × 10^{-9} ≈ −0.6 × 10^{-7} (compression).

4.3. SHGE in Average Daily Variations in Water Pressure in Well E-1

4.3.1. Hydrogeodynamic Precursor

Synchronous changes in water level and water pressure recorded by two sets of equipment during the EQ are shown in Figure 9, including the occurrence of hydrogeodynamic precursor HGP and post-seismic level/pressure rise within two months after the EQ.

The hydrogeodynamic precursor manifested itself for the 92 days before the EQ, starting from 1 January 2023 (Figure 9aB,aD,bB,bD). Before the EQ, the amplitude of the level decrease was −4.2 cm with an average daily rate of 0.00 to −0.30 cm/day. The amplitude of the water pressure decrease at a depth of 6 m below water level was −3.5 hPa with an average daily rate of 0.00 to −0.23 hPa/day.

Previously, the hydrogeodynamic precursor in water level changes in well E-1 was recorded in real time before the earthquakes of 28 February 2013, M_w = 6.9, d_e = 280 km; 30 January 2016, M_w = 7.2, d_e = 80 km; 16 March 2021, M_w = 6.6, d_e = 350 km and before some other seismic events [3–5,13,31,33]. According to the conclusions of KB REC, based on observations in well E-1 from 2002 to 2023, early successful forecasts were made of the location, time and magnitude of ten earthquakes with M_w = 5.6–7.2, including the 3 April 2023 earthquake.

The most probable mechanism for the occurrence of a hydrogeodynamic precursor during the preparation of EQ is an increase in the fracture-pore capacity of water-bearing rocks in the area of the well filter and the outflow of water from the wellbore into the rocks around the wellbore. Such a process is possible during the development of fracture dilatancy in low-porosity water-bearing rocks over a time interval of a day to tens of days before earthquakes. Previously, the determining role of fracture dilatancy in the formation of hydrogeochemical precursors in the composition of waters from self-flowing wells in the territory of Petropavlovsk–Kamchatsky geodynamic test site was indicated in [3,37]. The time of manifestation of hydrogeochemical precursors was 1-9 months, while the average time of hydrogeodynamic precursor in well E-1 is somewhat shorter and amounts to 43 days with a range of values from 8 to 70 days ([3], Explanation to Table S3 in Supplementary Materials).

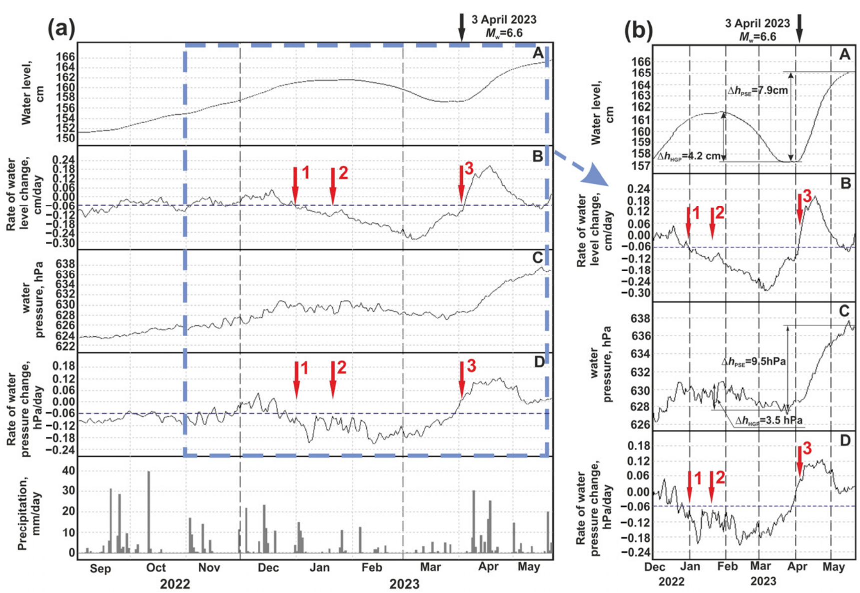

Figure 9. Well E-1: (**a**) water level (**A**), water pressure (**C**) and their average daily rate changes (**B**,**D**) due to the earthquake on 3 April 2023, M_w = 6.6 (EQ), compared to precipitation, September 2022–May 2023. EQ is indicated with a black arrow. In the graphs of the daily average rate of water level and water pressure variations, red arrows with numbers show the following: 1—1 January—

the onset of the hydrogeodynamic precursor, 2—19 January—the date of submission of a forecast report on a potential strong earthquake to KB REC, 3—3 April—earthquake, where the dashed line indicates the threshold of water level decrease rate. The bold dashed line outlines a fragment of observations, shown in the figure (**b**): (**A**)—water level and (**C**)—water pressure variations from 1 December 2022 to 30 May 2023, including hydrogeodynamic precursor and postseismic rise; (**B**,**D**)—average daily rate of water level and water pressure changes, respectively, in comparison with their threshold values.

4.3.2. Post-Seismic Effect

The post-seismic increase in water level and water pressure with amplitudes of 7.9 cm and 9.5 hPa and their subsequent stabilization continued for about two months (Figure 9aA,aC,bA,bC).

Considering that the amplitude of the post-seismic increase in water level/pressure in well E-1 was approximately two to three times greater than the amplitude of decrease in water level/pressure before the EQ (Figure 9bA,C), it can be assumed that two processes developed at the postseismic stage: (i) the inflow of underground water into the wellbore due to the restoration of fracture-pore capacity of water-bearing rocks and (ii) a decrease in the density of water in the wellbore and surrounding water-bearing rocks due to the transition of dissolved methane-nitrogen gas into a free state in the form of gas bubbles during seismic shaking.

In the case of EQ, the observed changes in water pressure in well E-1 corresponded to similar changes during other local strong (Mw ≥ 6.6) earthquakes at the epicentral distances of up to 300 km.

5. Discussion

5.1. Updated Typification of Seismo-Hydrogeodynamic Effects in Wells YuZ-5 and E-1

When creating the typification of SHGE for wells YuZ-5 and E-1, we took into account the main genetic types of SHGE [31]: (i) hydrogeodynamic precursors that appear at the stage of earthquake preparation; (ii) coseismic pressure jumps with changes in the static stress state of water-bearing rocks during the formation of rupture in the earthquake source (co-seismic effects CSE); (iii) co- and post-seismic effects during and after passage to seismic waves (PSE). The sequence of SHGE genetic types in groundwater pressure changes HGP → CSE → PSE reflects the staging of seismic influence on the state of the "well–aquifer" system during individual earthquakes and previously was observed in the wells of Kamchatka during strong ($M_w \geq 6.6$) local earthquakes, accompanied by tremors with an intensity of at least 4–6 points on the *MSK*-64 scale [3,31,33].

Figure 10 shows the distribution of different types of SHGEs diagnosed over the entire observation period in well YuZ-5 (Figure 10a) and well E-1 (Figure 10b), in comparison with the SHGE diagnosed during the EQ (highlighted in red). These diagrams were constructed using the data presented in Sections 3 and 4.

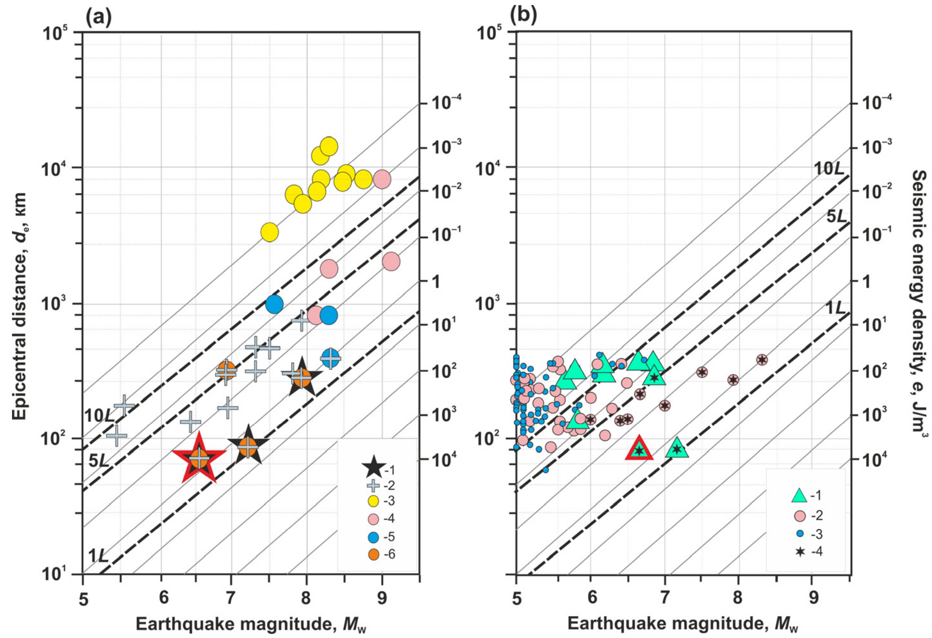

Figure 10. Distribution of various types of seismo-hydrogeodynamic effects in water level/pressure changes as functions of magnitude M_w, epicentral distance of earthquakes d_e and seismic energy density e. One, five and ten maximum linear sizes of earthquake sources as a function of magnitude M_w are shown as 1L, 5L and 10L. (**a**) In the YuZ-5 well: 1—supposed hydrogeodynamic precursor (EQ highlighted with a red thick contour line), 2—coseismic jumps (CSE), 3–6—vibration effects of seismic waves: 3—type I, 4—type II, 5—type III, 6—type IV (Table 5) [5,26]. (**b**) In well E-1: 1—hydrogeodynamic precursor (HGP) detected in real time, with the issuance of a conclusion on the possibility of an earthquake for KB REC, 2013–2023 (EQ highlighted with a red thick contour line); 2—precursor HGP before $M_w \geq 5.0$, $d_e \leq 360$ km earthquakes revealed retrospectively, 1987–2023; 3—no precursor HGP before $M_w \geq 5.0$, $d_e \leq 360$ km earthquakes, 1996–2023; 4—post-seismic rise in water level (PSE).

In the diagrams, constructed in the coordinates of magnitude M_w—epicentral distance of earthquakes to well d_e, the calculated values of seismic energy density in the observation area e (in J/m^3 according to [30]) and the maximum linear size of earthquake source L (in km, according to [41]) are shown with inclined lines depending on the values of M_w and d_e. This representation of the SHGE allows us to display in a compact form the relationship between registered effects in water pressure changes in an individual well and magnitude and spatial characteristics of seismic events causing such effects, and also to estimate the distances of the well from earthquake sources on the ratio between epicentral distances and linear size of the earthquake sources d_e/L. This approach significantly complements the general genetic typing of SHGE and specifies the features of seismo-hydrogeodynamic effect manifestations in individual wells.

Thus, the diagrams in Figure 10 represent the structure (model) of possible changes in groundwater pressure in two observation wells depending on earthquake parameters. Using the data in Figure 10, it is possible to give a meaningful description of the characteristic types of SHGEs that manifest themselves in well YuZ-5 (Figure 10a) and in well E-1 (Figure 10b) depending on the magnitude and spatial parameters of earthquakes accompanied by manifestations of certain types of SHGEs.

For example, according to observation data from 1997–2022, the supposed hydrogeodynamic precursors appeared in well YuZ-5 before ZhE and KE earthquakes with M_w = 7.2 and 7.8 (L_{ZhE} = 76 km and L_{KE} = 139 km) at epicentral distances d_e = 86 and d_e = 200 km (d_e/L = 1.1–1.4). The intensity of seismic impact in the well area during these earthquakes was I_{MSK-64} = 5–6 points with values of e = 0.4 and 4 J/m^3. These two earthquakes were accompanied, in addition to the supposed hydrogeodynamic precursors, by the manifestation of coseismic jumps in water pressure changes (CSE) and long-term postseismic decreases in water pressure, corresponding to type IV of vibration impact of seismic waves [5,26].

The EQ, with comparable values of parameters M_w = 6.6, d_e = 67 km, as well as values of the intensity of seismic impact in well area e = 0.6 J/m^3, I_{MSK-64} = 5–6 points, was accompanied by a similar set of seismo-hydrogeodynamic effects (Figures 6 and 8). The EQ is characterized by the ratio of epicentral distance to the size of earthquake source d_e/L = 1.6, which shows the location of well YuZ-5 in the near-intermediate zone of the earthquake source as well as in the cases of the Kronotsky and Zhupanovsky earthquakes.

Thus, these three earthquakes (EQ together with KE and ZhE) can be considered as a special class of earthquakes, in which a full set of genetic types of seismo-hydrogeodynamic effects can be manifested in well YuZ-5 and for which, with more reliable confirmation of the supposed hydrogeodynamic precursor, there is the potential for their early prediction.

From the diagram in Figure 10a, one can also obtain the parameters of earthquakes accompanied by coseismic pressure jumps (CSE) and various types of vibration effects (PSE) in well YuZ-5.

Figure 10b presents for the first time a refined typification of seismo-hydrogeodynamic effects for well E-1, including the SHGEs recorded during the EQ (see Section 4.3). In well E-1, the main types of SHGEs are the hydrogeodynamic precursor HGP and post-seismic increase in water level/pressure followed by stabilization. From this diagram, it follows that the HGP appears before earthquakes with magnitudes $M_w \geq 5.0$ at epicentral distances d_e = 70–360 km. Before earthquakes with magnitudes M_w = 5.0–6.5, HGP was observed in approximately 50% of cases. Before earthquakes with magnitudes M_w = 6.6–8.3, HGP was observed in 100% of cases. The presented estimates of the relationship between the HGP and subsequent earthquakes, depending on their parameters, correspond to the case of the 3 April 2023 earthquake and the results of previous studies of this type of hydrogeodynamic precursor [3,31]. A gradual increase in water pressure with an amplitude of ≈8 cm over two months after the EQ (Figure 9) is a typical post-seismic effect in this well, observed in connection with local strong earthquakes, most of which had Mw ≥ 6.6 and occurred at distances of no more than 200 km from the well.

The diagrams for two Kamchatka wells presented in Figure 10 are important evidence of significant differences between individual observation wells in sensitivity to earthquakes with different parameters. As can be seen from the comparison of the SHGE typification diagrams, well YuZ-5 is more "sensitive" to remote earthquakes. This well recorded the vibration effects of seismic waves from strong earthquakes at distances of up to 14 thousand km. On the other hand, the "sensitivity" of well E-1 is limited to distances of about 200 km in relation to the impact of seismic waves from strong local earthquakes. For well E-1, according to the manifestation of HGP, the zone of sensitivity to the preparation of local earthquakes with $M_w \geq 5.0$ is limited to epicentral distances of no more than 360 km.

The creation of such diagrams for individual observation wells, similar to Figure 10, together with the description of registered seismo-hydrogeodynamic effects depending on earthquake parameters, is a necessary element when using well observations in earthquake prediction and studying the influence of seismicity on groundwater. Such reliably confirmed SHGE typifications for individual wells characterize the expected variations in water pressure, as well as other groundwater parameters, during corresponding observations. A compact description of the seismo-hydrogeodynamic effects in the form of typification diagrams allows for an advanced forecast of expected seismo-hydrogeodynamic effects during individual earthquakes depending on their parameters.

At the same time, to obtain quality data for creating such typifications, especially in relation to local strong earthquakes, precision observations over a long time, not less than decades, are necessary. For example, in the case of well YuZ-5, a complete set of SHGEs was obtained during the Kronotsky earthquake on 5 December 1997, $M_w = 7.8$, which occurred three months after the start of precision observations in September 1997. However, confirmation of precisely this set of SHGEs—the supposed precursor–coseismic pressure jump–post-seismic pressure drop as a manifestation of type IV vibration impact of seismic waves—became possible only 18 years later during the Zhupanovsky earthquake on 30 January 2016 $M_w = 7.2$, and also 8 years later during the 3 April 2023 earthquake under consideration.

In order to significantly reduce the time required to create SHGE typifications for individual wells, it is possible to use both direct data on registered seismo-hydrogeodynamic effects and the analogy method using data on local geological and hydrogeological conditions, the technical structure of the well, barometric and tidal responses of water pressure in the well under study and a comparison of these data with other wells that have been better studied in relation to the influence of seismicity. We consider the development of criteria for comparing different wells for the creation of the SHGE typifications as a promising direction for further research.

For wells 1303 and M-1, the duration of precision observations is relatively short (Table 1). We have only begun to collect information on seismo-hydrogeodynamic effects for the subsequent creation of the SHGE typification diagrams for these wells. The registration of SHGEs in these wells from the strongest remote earthquakes (Section 3.3) shows their high sensitivity to the impact of surface seismic waves, similar to the sensitivity of well YuZ-5. The detection of a coseismic pressure jump in well 1303 during EQ allows us to hope for diagnostics of such co-seismic effects in this well during other local earthquakes. In terms of assessing coseismic deformations during strong local earthquakes, well 1303 can be considered a certain analogue of well YuZ-5.

5.2. Lessons from the 3 April 2023 Earthquake

The description of seismo-hydrogeodynamic effects in Kamchatka observation wells in connection with the EQ confirms, in general, the previously created typifications of the SHGEs for wells YuZ-5 and E-1. Using the example of the EQ, a certain repeatability of the sequence of the genetic types of the SHGEs during the strongest local earthquakes in well YuZ-5 (the supposed hydrogeodynamic precursor $\rightarrow$ CSE $\rightarrow$ PSE) and in the well E-1 (HGP $\rightarrow$ PSE) was also traced.

On the other hand, the EQ was the first strong seismic event after upgrading the equipment [4] and obtaining precision high-frequency records of water pressure with a frequency of 1 Hz in wells YuZ-5, 1303, M-1, as well as records of pressure, temperature and electrical conductivity of water with a frequency of 2 min in well E-1. As a result, observation data were obtained on new short-term manifestations of hydrogeodynamic effects (Figure 6) and effects on changes in pressure, temperature and electrical conductivity of water in well E-1 (see Section 4.2.1) arising during the passage of intense body seismic waves and tremors with an intensity of $I_{msk\text{-}64} = 5$–6 points. Such data, if they are reliably verified in the future, can form a factual basis for the development of the typification of the SHGEs in terms of identifying the new vibration effects of seismic waves.

5.3. About Hydrogeodynamic Precursors and Forecast of the 3 April 2023 Earthquake

We have described two types of hydrogeodynamic precursors that appeared in wells YuZ-5 and E-1 before the 3 April 2023 earthquake. Therefore, it is necessary to make clarifications regarding their practical significance for earthquake forecasting.

In well YuZ-5 during the 2.5 months before the EQ, increased values of water pressure, with the most noticeable increase from mid-January to mid-February 2023, exceeding the seasonal pressure by 10.2 hPa, were identified retrospectively (Figure 8b). We assume that such an excessive increase in groundwater pressure in relation to the average seasonal head pressure could be a manifestation of the EQ hydrogeodynamic precursor by analogy with the manifestations of the supposed precursors before the KZ and ZhE.

Despite the repeated manifestation of this type of the supposed precursor during the period from 20 days to 3 months before earthquakes with amplitudes of deviation of current data from the average seasonal pressure function of 10.2–30 cm of the water column, we are somewhat cautious about its use in real-time earthquake forecasting for the following reasons:

(i) All manifestations of the supposed precursor approximately corresponded to or slightly exceeded the average error in determining the average seasonal pressure function (±10 cm), i.e., the statistical significance of the retrospective diagnosis of this precursor is relatively small.

(ii) All three manifestations of the precursor fall on the transition period from the autumn hydrological maximum to the winter minimum, the individual characteristics of which can vary greatly in different years depending on the total autumn precipitation [5].

The above circumstances, as well as the complex relationship of hydrostatic pressure change with the intensity of atmospheric precipitation, leave reasonable doubts about the possibility of reliably identifying this type of precursor based on the current observation data in well YuZ-5.

We presented data on the supposed precursor in the water pressure change in well YuZ-5 and the corresponding estimates of the quasi-elastic deformation of water-bearing rocks at the preparation stages of all three strong seismic events, amounting to 0.7–1.9 × 10^{-7} (see Sections 3.2.1 and 4.2.3), taking into account the data on various seismic and hydrogeochemical precursors, as well as the manifestation of the precursor HGP in well E-1 before these large seismic events [3,31,33,37]. We believe that the descriptions of the supposed hydrogeodynamic precursors in well YuZ-5 may be useful for further study of earthquake precursors in Kamchatka.

Another situation occurs with the hydrogeodynamic precursor HGP in the water level/pressure changes in well E-1. The empirically determined recurrence of HGP before earthquakes with $M_w \geq 5.0$ at epicentral distances $d_e \leq 360$ km (more than 70% of such earthquake cases), as well as the improvement of the statistical relationship of the HGP with subsequent earthquakes with an increase in their magnitude (see Section 3.1.1), made it possible to use HGP for medium-term (first tens of days to weeks) assessment of the time of local strong earthquake occurrences [3,13,31].

Since 2002, based on current observations at well E-1, conclusions have been drawn up weekly on the presence/absence of HGP. Such conclusions are transferred to the KB REC. When HGP is detected in water level/pressure changes, the conclusion provides rough estimates of the time (from several days to 1–2 months), location (≤360 km from the well) and magnitude ($M_w \geq 5.0$) of the expected earthquake based on the retrospective analysis of the relationship between HGP and earthquakes (Figure 10b) ([3], Supplementary Material, Table S3). If no precursor is detected in the water level changes, the report states “there is no precursor”. Thus, the conclusions submitted to the Expert Council can be divided into two categories:

(i) conclusions containing a certain concern regarding the increase in the danger of a strong earthquake;
(ii) conclusions that do not increase the concern regarding a strong earthquake.

Therefore, such conclusions are useful in the expert method of analyzing a set of seismic forecast data available to the Council on a certain date.

According to the KB REC conclusions, for the period from 2002 to 2023, based on the HGP identified in real time in the water level changes in well E-1, successful forecasts of ten earthquakes with M_w = 5.6–7.2 (Figure 10b) were made, including four forecasts of the earthquakes with magnitudes M_w = 6.4–7.2 occurring at epicentral distances of 80–350 km [9,42].

Using the HGP identified in real time (Figure 9), on 19 January 2023, a forecast conclusion was prepared on the increased probability of a strong earthquake, which was transmitted to the KB REC. The conclusion of January 19, 2023 stated: "Over the course of 14 days, an alarming sign of HGP has been manifested in the water pressure changes in well E-1. This indicates that within 1–2 months an earthquake with $M_w \geq 5.0$ is possible at a distance of up to a few hundred kilometers from the well.".

Over time, from the third decade of January to March 2023, this forecast was confirmed weekly by the authors.

The 3 April 2023 EQ with M_w = 6.6 roughly corresponded to the wording of the forecast from January 19 in terms of magnitude ($M_w \geq 5.0$), time (waiting time from 19 January to 3 April is 75 days or 2.5 months ≈ 2 months) and location (epicentral distance to well E-1 d_e = 77 km). Therefore, this forecast, according to the authors' opinion, as well as according to the conclusion of the KB REC, is successful.

We believe that such predictive estimates of the development in local seismicity on the well observation data are particularly useful in forecasts of the timing of strong earthquakes accompanied by noticeable tremors, as in the case of the 3 April 2023 earthquake. The presented long-term experience in forecasting individual strong earthquakes based on the hydrogeodynamic precursor identified in real time by the changes in water pressure in well E-1 is unique. This example shows the need for experimental forecasting of earthquakes using different retrospectively identified alarm signals in current well observation data in other seismically active regions.

6. Conclusions

This paper summarizes the results of long-term (1996–2023) precision well observations on the Kamchatka Peninsula, which were conducted by the authors to search for hydrogeodynamic precursors of strong earthquakes, develop seismic forecasting methods and study the impact of seismicity on groundwater. The main methods of our research were:

(i) ensuring high quality of experimental data on water level/pressure recording;
(ii) systematization of data on seismo-hydrogeodynamic effects in individual wells depending on earthquake parameters;
(iii) experimental forecasting of individual strong earthquakes based on the hydrogeodynamic precursor in water level changes in well E-1 for which retrospective estimates of prognostic effectiveness were obtained for the entire observation period (Table 4);
(iv) conducting an experiment since 2002 on the use of the hydrogeodynamic precursor (HGP) to predict earthquakes in real time by submitting forecasts to the Kamchatka branch of the Russian Expert Council for Earthquake Forecasting and Seismic Hazard and Risk Assessment (KB REC).

The paper demonstrates that one of the tasks of long-term well observations carried out for seismic forecasting is to verify the relationships between the various types of seismo-hydrogeodynamic effects in observation wells with earthquake parameters. Such verification of knowledge about the SHGEs manifested in individual wells during the most dangerous local earthquakes can be carried out when strong local earthquakes occur and the recorded effects in water pressure changes are compared with the previously recorded effects for earthquakes with similar parameters.

Using the example of the 3 April 2023 earthquake, M_w = 6.6, which occurred at the epicentral distance of about 70–80 km from the observation wells, the following is shown:

(i) The well observation system in the east of Kamchatka Peninsula makes it possible to diagnose in near real time various types of seismo-hydrogeodynamic effects manifested in groundwater pressure changes in the range of periods from seconds to minutes to tens of days, including hydrogeodynamic precursors.
(ii) The registered SHGEs in observation wells, in general, corresponded to the expected sequence of the main genetic types of SHGEs: hydrogeodynamic precursors, co- and postseismic effects of static changes in the stress state of water-bearing rocks and the dynamic impact of seismic waves.
(iii) Individual observation wells are characterized by a unique set and specific forms of SHGE manifestations, which are repeated during earthquakes with similar parameters.

A compact representation of various types of SHGEs in individual wells depending on earthquake parameters in the form of SHGE typification diagrams using the example of wells YuZ-5 and E-1 is proposed and demonstrated (Figure 10). Presentation of the SHGE data in the form of diagrams (Figure 10) allows the use of such diagrams to assess changes in water pressure in individual observation wells during various earthquakes depending on their parameters. Such diagrams are also useful for earthquake prediction based on hydrogeodynamic precursors and for general assessment of the impact of seismicity on groundwater based on well observation.

Using a hydrogeodynamic precursor identified in real time in water level/pressure changes in well E-1, the 3 April 2023 earthquake was predicted 75 days in advance and was confirmed by the authors' weekly reports during the period from January 19 until the EQ in accordance with the development of the hydrogeodynamic precursor (Figure 9). The successful earthquake prediction was confirmed by the Specialized Expert Council for Earthquake Forecasting (KB REC).

For well YuZ-5, it is possible to assume a sequence of manifestation of seismo-hydrogeodynamic effects HGP → CSE → PSE during the three strongest and closest local earthquakes, including the EQ. Parameters of such earthquakes M_w = 6.6–7.8, d_e = 70–200 km and their impact in the well area e = 4.0–0.4 J/m^3, $I_{MSK\text{-}64} \geq$ 5–6 points are estimated. For all three earthquakes, the observation well was located in the near-intermediate zone of the earthquake sources (d_e/L = 1.1–1.6) (Figure 10a). However, confirmation of the correctness of the proposed SHGE typification for this well in relation to supposed hydrodynamic precursors requires further research and more convincing examples of their manifestation.

The presented experience of observing a set of seismo-hydrogeodynamic effects in connection with the EQ confirmed substantially the correctness of the SHGE typifications depending on the parameters of earthquakes for wells YuZ-5 and E-1.

The recording of coseismic pressure jumps (coseismic effect—CSE) in wells YuZ-5 and 1303 during the EQ and the obtained estimates of the volumetric coseismic deformation of water-bearing rocks (expansion with amplitude of D_1 = (0.7–1.0) × 10^{-8}), consistent with theoretical estimates based on the dislocation model [35], demonstrate the possibility of using data from these wells to obtain quantitative estimates of the quasi-elastic deformation of water-bearing rocks in the study of both modern geodynamic processes and hydrogeodynamic earthquake precursors in the Kamchatka region.

Author Contributions: G.K. and S.B. have made a substantial, direct and intellectual contribution to the work. All authors have read and agreed to the published version of the manuscript.

Funding: The work was supported by Ministry of Science and Higher Education of the Russian Federation (075-00604-25). The data used in the work were obtained with large-scale research facilities "Seismic infrasound array for monitoring Arctic cryolitozone and continuous seismic monitoring of the Russian Federation, neighbouring territories and the world" (http://www.gsras.ru/unu/about.html (accessed on 5 February 2025)).

Data Availability Statement: The original contributions presented in this study are included in the article; further inquiries can be directed to the corresponding author. All well observation data are contained in the KB GS RAS database http://www.gsras.ru/new/infres/ (accessed on 5 February 2025) and can be obtained by interested parties upon request.

Conflicts of Interest: The authors declare that this research was conducted in the absence of any commercial or financial relationships that could be construed as a potential conflict of interest.

References

1. Wang, C.-Y.; Manga, M. *Earthquakes and Water*; Lecture Notes in Earth Sciences; Springer: Berlin, Germany, 2010; p. 225. https://doi.org/10.1007/978-3-642-00810-8.
2. Wang, C.-Y.; Manga, M. *Water and Earthquakes*; Lecture Notes in Earth System Sciences; Springer: Cham, Switzerland, 2021; p. 387. https://doi.org/10.1007/978-3-030-64308-9.
3. Kopylova, G.N.; Boldina, S.V. Hydrogeological Earthquake Precursors: A Case Study from the Kamchatka Peninsula. *Front. Earth Sci*. **2020**, *8*, 576017. https://doi.org/10.3389/feart.2020.576017.
4. Boldina, S.V.; Kopylova, G.N.; Kobzev, V.A. Study of Seismic Effects on Changes in Groundwater Pressure: Equipment and Some Well Observastion Results for the Kamchatka Peninsula. *Geodyn. Tectonophys.* **2022**, *13*, 0594. https://doi.org/10.5800/GT-2022-13-2-0594. (In Russian)
5. Kopylova, G.; Boldina, S. Seismo-Hydrogeodynamic Effects in Groundwater Pressure Changes: A Case Study of the YuZ-5 Well on the Kamchatka Peninsula. *Water*. **2023**, *15*, 2174. https://doi.org/10.3390/w15122174.
6. Sheymovich, V.S. *Explanation to the State Geological Map of the Russian Federation. Scale 1:200,000. Series South Kamchatka*; VSEGEI: Moscow, Russia, 2000; p. 302. (In Russian)
7. Kiryukhin, A.; Lavrushin, V.; Kiryukhin, P.; Voronin, P. System of Koryaksky–Avachinsky Volcanoes (Kamchatka, Russia). *Geofluids* **2017**, *2017*, 4279652. https://doi.org/10.1155/2017/4279652.
8. Taran, Y.; Ryabinin, G.; Pokrovsky, B.; Malik, N.; Cienfuegos, E. Methane–rich thermal and mineral waters of the Avachinsky Depression, Kamchatka. *Appl. Geochem.* **2022**, *145*, 105414. https://doi.org/10.1016/j.apgeochem.2022.105414.
9. Chebrov, V.N.; Saltykov, V.A.; Serafimova, Y.K. Identifying the Precursors of Large ($M \geq 6.0$) Earthquakes in Kamchatka Based on Data from the Kamchatka Branch of the Russian Expert Council on Earthquake Prediction: 1998–2011. *J. Volcanol. Seismol.* **2013**, *7*, 76–85. https://doi.org/10.1134/S074204631301003X.
10. Riznichenko, Y.V. The source dimensions of the crustal earthquakes and the seismic moment. In *Issledovaniya po Fizike Zemletryasenii (Studies in Earthquake Physics)*; Nauka: Moscow, Russia, 1976; pp. 9–27. (In Russian)
11. Gordeev, E.I.; Pavlov, V.M. Subduction of the Pacific plate under Kamchatka: Seismic velocity of underthrust. *Izv. Phys. Solid Earth* **2009**, *45*, 326–337. https://doi.org/10.1134/S1069351309040053.
12. Gordeev, E.I.; Pinegina, T.K.; Lander, A.V.; Kozhurin, A.I. Beringia: Seismic Hazard and Fundamental Problems of Geotectonics. *Izv. Phys. Solid Earth* **2015**, *51*, 512–521. https://doi.org/10.1134/S1069351315030039.
13. Kopylova, G.N.; Boldina, S.V. On the Relationships of Water-Level Variations in the E-1 Well, Kamchatka to the 2008–2009 Resumption of Activity on Koryakskii Volcano and to Large ($M \geq 5$) Earthquakes. *J. Volcanol. Seismol.* **2012**, *6*, 316–328. https://doi.org/10.1134/S074204631205003X.
14. Rojstaczer, S. Determination of fluid flows properties from the response of water levels in wells to atmospheric loading. *Water Resour. Res.* **1988**, *24*, 1927–1938.
15. Van der Kamp, G.; Gale, L.E. Theory of Earth tide and barometric effects in porous formations with compressible grains. *Water Resour. Res.* **1983**, *19*, 538–544.

16. Rojstaczer, S.; Agnew, D. The influence of formation material properties on the response of water levels in wells to earth tides and atmospheric loading. *J. Geophys. Res.* **1989**, *94*, 12403–12411.
17. Igarashi, G.; Wakita, H. Tidal responses and earthquake-related changes in the water level of deep wells. *J. Geophys. Res*. **1991**, *96*, 4269–4278.
18. Roeloffs, E. Persistent water level changes in a well near Parkfield, California, due to local and distant earthquakes. *J. Geophys. Res.* **1998**, *103*, 869–889.
19. Chia, Y.; Chiu, J.-J.; Chiang, Y.-H.; Lee, T.-P.; Wu, Y.-M.; Horng, M.-J. Implications of coseismic groundwater level changes observed at multiple-well monitoring stations. *Geophys. J. Int.* **2008**, *172*, 293–301. https://doi.org/10.1111/j.1365-246X.2007.03628.x.
20. Shi, Z.; Wang, G.; Liu, C. Co-seismic groundwater level changes induced by the May 12, 2008 Wenchuan earthquake in the near field. *Pure Appl. Geophys*. **2013**, *170*, 1773–1783. https://doi.org/10.1007/s00024-012-0606-1.
21. Shi, Z.; Wang, G.; Manga, M.; Wang, C.-Y. Mechanism of co–seismic water level change following four great earthquakes—Insights from co-seismic responses throughout the Chinese mainland. *Earth Planet. Sci. Lett.* **2015**, *430*, 66–74. https://doi.org/10.1016/j.epsl.2015.08.012.
22. Sun, X.; Wang, G.; Yang, X. Coseismic response of water level in Changping well, China, to the M_w 9.0 Tohoku earthquake. *J. Hydrol.* **2015**, *531*, 1028–1039. https://doi.org/10.1016/j.jhydrol.2015.11.005.
23. Zhang, S.; Shi, Z.; Wang, G.; Zhang, Z. Quantitative Assessment of the Mechanisms of Earthquake–Induced Groundwater–Level Change in the MP Well, Three Gorges Area. *Pure Appl. Geophys.* **2018**, *175*, 2475–2484. https://doi.org/10.1007/s00024-017-1643-6.
24. Shalev, E.; Kurzon, I.; Doan, M.-L.; Lyakhovsky, V. Sustained water-level changes caused by damage and compaction induced by teleseismic earthquakes. *J. Geophys. Res. Solid Earth* **2016**, *121*, 4943–4954. https://doi.org/10.1002/2016JB013068.
25. Shalev, E.; Kurzon, I.; Doan, M.-L.; Lyakhovsky, V. Water–level oscillations caused by volumetric and deviatoric dynamic strains. *Geophys. J. Int*. **2016**, *204*, 841–851. https://doi.org/10.1093/gji/ggv483.
26. Kopylova, G.N.; Boldina, S.V. Effects of Seismic Waves in Water Level Changes in a Well: Empirical Data and Models. *Izv. Phys. Solid Earth* **2020**, *56*, 530–549. https://doi.org/10.1134/S1069351320030039.
27. Kopylova, G.N.; Steblov, G.M.; Boldina, S.V.; Sdel'nikova, I.A. The possibility of estimating the coseismic deformation from water level observations in wells. *Izv. Phys. Solid Earth* **2010**, *46*, 47–56. https://doi.org/10.1134/S1069351310010040.
28. Xiang, Y.; Sun, X.; Gao, X. Different coseismic groundwater level changes in two adjacent wells in a fault-intersected aquifer system. *J. Hydrol*. **2019**, *578*, 124123. https://doi.org/10.1016/j.jhydrol.2019.124123.
29. Lyubushin, A.A.; Kazantseva, O.S.; Manukin, A.B. Analysis of Long-Term Observations of the Groundwater Level in an Aseismic Region. *Izv. Phys. Solid Earth* **2019**, *55*, 232–249. https://doi.org/10.1134/S106935131902006X.
30. Wang, C.-Y. Liquefaction beyond the near field. *Seismol. Res. Lett.* **2007**, *78*, 512–517. https://doi.org/10.1785/gssrl.78.5.512.
31. Kopylova, G.N.; Boldina, S.V. Seismohydrogeological Phenomena as an Earthquake's Trigger Impact on Groundwater (by the Example of the Wells of the Petropavlovsk-Kamchatsky Test Site, Kamchatka Peninsula. *Izv. Phys. Solid Earth* **2023**, *59*, 405–420. https://doi.org/10.1134/S1069351323030072.
32. Gusev, A.A. Earthquake prediction based on seismicity statistics. In *Seismichnost' i Seismicheskii Prognoz, Svoistva Verkhnei Mantii i ikh Svyaz' s Vulkanizmom na Kamchatke (Seismicity and Earthquake Prediction, Upper Mantle Properties and Their Relationship to Volcanism in Kamchatka)*; Novosibirsk: Nauka, Russia, 1974; pp. 109–119. (In Russian).
33. Boldina, S.V.; Kopylova, G.N. Effects of the January 30, 2016, $M_w = 7.2$ Zhupanovsky earthquake on the water level variations in wells YuZ-5 and E-1 in Kamchatka. *Geodyn. Tectonophys.* **2017**, *8*, 863–880. https://doi.org/10.5800/GT-2017-8-4-0321. (In Russian)
34. Medvedev, S.V.; Sponheuer, W.; Kárník, V. *Seismic Intensity Scale MSK-64*; Akad. Nauk SSSR, Geofiz. Kom: Moscow, Russia, 1965; p. 11. (In Russian)
35. Okada, Y. Surface deformation due to shear and tensile faults in a half–space. *Bull. Seismol. Soc. Am.* **1985**, *75*, 1135–1154.
36. Cooper, H.H.; Bredehoeft, J.D.; Papadopulos, I.S.; Bennet, R.R. The response of well-aquifer system to seismic waves. *J. Geophys. Res.* **1965**, *70*, 3915–3926.
37. Kopylova, G.N.; Boldina, S.V.; Serafimova, Y.K. Earthquake Precursors in the Ionic and Gas Composition of Groundwater: A Review of World Data. *Geochem. Int.* **2022**, *60*, 928–946. https://doi.org/10.1134/S0016702922100056.
38. Brodsky, E.E.; Roeloffs, E.; Woodcock, D.; Gall, I.; Manga, M.A. A Mechanism for sustained groundwater pressure changes induced by distant earthquakes. *J. Geophys. Res.* **2003**, *108*, 2390–2400. https://doi.org/10.1029/2002JB002321.
39. Crank, J. *The Mathematics of Diffusion*; Oxford Sci.: Oxford, UK, 1975; p. 421.

40. Freeze, R.A.; Cherry, J.A. *Groundwater*; Prentice-Hall: Englewood Cliffs, NJ, USA, 1979; p. 604.
41. Zavyalov, A.D.; Zotov, O.D. A new way to determine the characteristic size of the source zone. *J. Volcanol. Seismol.* **2021**, *15*, 19–25. https://doi.org/10.1134/S0742046321010139.
42. Chebrov V.N.; Abubakirov I.R.; Bogdanov V.V.; Boldina S.V.; Buss Yu.Yu.; Vlasov Yu.A.; Gavrilov V.A.; Gasheva O.A.; Gusev A.A.; Guseva E.M.; et.al. *Sil'nye Kamchatskie Zemletryaseniya 2013 Goda (Strong Earthquakes of Kamchatka in 2013)*; Chebrov, V.N., Ed.; Novaya Kniga: Petropavlovsk-Kamchatsky, Russia, 2014; p. 252. (In Russian)